Glacier Mass Balance and Its Response to 2022 Heatwaves for Kangxiwa Glacier in the Eastern Pamir: Insights from Time-Lapse Photography ~~and In-situ Measurements~~

Ying Xie[1,2], Baiqing Xu[1,2], Meilin Zhu[3], Yu Fan[1,4], Pengling Wang[5], Song Yang[6], Wenqing Zhao[1,4], Wei Yang[1,2*]

[1]State Key Laboratory of Tibetan Plateau Earth System, Environment and Resources (TPESER), Institute of Tibetan Plateau Research, Chinese Academy of Sciences, Beijing 100101, China
[2.] Muztagh Ata Station for Westerly Environment Observation and Research, Chinese Academy of Sciences, China
[3] College of Earth and Environmental Sciences, Lanzhou University, Lanzhou 730000, China
[4] College of Resources and Environment, University of Chinese Academy of Sciences, Beijing 100049, China
[5.]National Climate Centre, China Meteorological Administration, Beijing 100081, China
[6] School of Geographical Sciences, China West Normal University, Nanchong 637009, China

Correspondence to: Wei Yang (yangww@itpcas.ac.cn)

Abstract. Contrary to the widespread glacier mass loss in High Mountain Asia under global warming, glaciers in the Pamir-Karakoram region have exhibited anomalously less negative mass ~~changes~~ balances and even slight mass gains in recent decades. While geodetic studies have quantified decadal-scale mass loss, the process of glacier mass balance and its response to ~~regional climate~~extreme climate events ~~change~~ remain poorly understood due to the scarcity of high ~~-~~temporal ~~-~~resolution of mass ~~change~~balance observations. This study ~~analyzes~~analyses the characteristics of daily glacier mass balance during the period from 2019/2020 to 2022/2023 ~~-~~and their responses to the 2022 heatwaves based on time-lapse photography, ablation stake/snow pit measurements and nearby meteorological ~~data~~ records~~ed~~ collected at the Kangxiwa Glacier in the eastern Pamir. Our results showed that the Kangxiwa Glacier experienced weak mass loss in ~~2019/2000~~2019/2020 and 2020/2021 balance years ~~but~~ and significant mass deficits in 2021/2022 and 2022/2023. Observations ~~evidence~~ show that the Kangxiwa Glacier is a spring-accumulation and summer-ablation type, with spring (April-June) accumulation of ~~+~~200-~~500~~ 295 mm w.e. and summer (July-September) mass loss of ~~300~~306-~~900~~ 884 mm w.e during the past four years. The ~~unprecedented~~ heatwaves in July-August 2022 caused an abnormal mass loss of over ~~852~~ 800 mm w.e. within 40 days, ~~advancing the Glacier Mass Loss Day which was defined as the date when the net mass balance transitions to negative~~ depleting all ~~and all~~ winter snow accumulation ~~is depleted by~~ one month earlier and driv~~push~~ing the equilibrium line altitude above the glacier summit~~s~~. ~~The 2022 heatwaves, c~~Characterized by we~~a~~kened westerly circulation, the 2022 heatwaves likely ~~influenced~~ affected not only the ~~East~~ eastern Pamir region but also the western Kunlun Mountains, leading to increased incoming radiation and reduced precipitation. Our ~~studies~~ finding revealed that short-term heatwaves can trigger~~lead~~ substantial glacier mass loss in the ~~E~~eastern Pamir,~~the high-elevation glaciers in eastern Pamir are sensitive to the heatwaves,~~ once considered climate-resilient, suggesting that "Pamir–Karakorum" anomaly is increasingly challenged by the ~~rising~~growing frequency of

extreme heat events.~~the termination of the so-called Karakoram anomaly may reflect recent climatic warming in this high-elevation region.~~

1. Introduction

Under global climate warming, glaciers on Tibetan Plateau and its surrounding regions have suffered from significant mass loss over recent decades (Brun et al., 2017; Bhattacharya et al., 2021; Hewitt., 2011;~~-~~ Hugonnet et al., 2021; Shean et al., 2020). However, the notable exception, called the "Pamir–Karakorum" anomaly, observed~~occurred~~ in the western Kunlun, Karakoram and the eastern Pamir ranges, where glaciers have remained in balance or experienced slight mass gains since at least the 1970s (Hewitt~~Hewiit~~ et al., 2011; Berthier and Brun, 2019; Brun et al., 2017; Kääb et al., 2015). Recent studies suggested that this anomaly ~~maybe be~~might be transitioning to a generalized thinning, indicating the end of the "~~'~~Pamir–Karakorum"~~'~~ anomaly (Hugonnet et al., 2021).

Glaciers in Central Asia are a critical component of the hydrological cycle, providing substantial runoff during the dry summer months for agriculture or hydropower (Huss and Hock, 2018). In-depth analysis of glacier mass changes and their climate response is therefore essential for water resource management and regional sustainability. Geodetic studies have successfully determined decadal glacier mass changes (Shean et al., 2020; Hugonnet et al., 2021). However, the heterogeneous climatic and topographical conditions across the Tibetan Plateau and surroundings result in high spatial variability in glacier mass balance (Brun et al., 2019; Barandun et al., 2021; Barandun and Pohl, 2023; Zhu et al., 2023). In addition, long-term glaciological measurements are scarce across the western Tibetan Plateau, particularly in the western Kunlun, the Pamir and Karakoram ranges (Barandun and Pohl, 2023; Yao et al., 2022; Zemp et al, 2023). Direct glaciological measurements using ablation stakes and snow pits enable the derivation of seasonal and annual mass balance, supporting model calibration and validation (Cogley et al, 2011; Kaser et al, 2003~~Zhu et al., 2018; Ren et al., 2018~~). The limited availability of in-situ observations and detailed analysis of physical ablation and accumulation process has hindered a comprehensive understanding of the factors driving ~~these~~ glacier mass changes in this region~~dynamics~~.

~~Recent e~~Extreme events such as heatwaves ~~and droughts~~ have caused abnormal high-elevation melting in the world (Chen et al., 2023; Gui et al., 2024; Hassan et al., 2024; Little et al., 2019), threatening water security and triggering glacier~~-~~-related disasters (Kääb et al., 2018; Shugar et al., 2021; Zhao et al., 2022). For example~~s~~, a 25~~-~~-day heatwave in Switzerland in 2022 caused melt equivalent to 35% of the total summer ablation (Cremona et al., 2023). Similarly, the 2022 heatwave induced unexpected melting on the central Tibetan Plateau (Zhu et al., 2024a~~3~~; Zhu et al., 2024b) and severe mass loss at Urumqi Glacier No. 1 in the eastern Tien Shan (Xu et al., 2024). The increasing intensity, frequency and duration of regional extreme ~~events~~ heatwaves around the world pose a significant threat to mountain glaciers (~~Oliver et al., 2018;~~ Colucci et al., 2017; Perkins-Kirkpatrick and ~~others~~Lewis, 2020). ~~Traditional~~ The glaciological method and geodetic ~~survey~~

mass balance method can provide mass balance data at multi-year, annual, and seasonal scales. However, both approaches face challenges in capturing the high temporal ~~resolution~~ evolution of surface mass balance ~~dynamics differences~~, limiting our understanding of glacier responses to short-term ~~extreme events~~extreme events.

Recent advancements in high temporal resolution monitoring techniques to monitor ablation, such as the SmartStake by rolling the steel wire up~~steel wire anchored below the ice surface~~ (A2PS contributors 2021), automated cameras monitoring colour-coded ablation stakes (Landmann et al., 2021; Cremona et al., 2023), and terrestrial laser scanning techniques (Voordendag et al., 2023), have provided new insights into short-term surface mass balance variations, including their response to ~~the~~ extreme melt events (Cremona et al., 2023). New indices like the Glacier Loss Day (GLD), which was defined as the day when net mass balance becomes negative and winter snow is exhausted (Voordendag et al., 2023), have provided~~been developed to characterized the glacier climate imbalance~~ new insights into short-term mass balance variations~~, including their response to extreme melt events (Cremona et al., 2023)~~. In the summer of 2022, heatwaves swept across many parts of the Northern Hemisphere, causing extreme heat events in North America, Europe, and the Yangtze River in China (Lu et al., 2022). However, the processes and mechanisms through which these heatwaves impact glaciers in the eastern Pamir—long considered climatically stable—remain poorly constrained. To address this critical knowledge gap, this study prioritizes time-lapse camera observations to capture daily surface mass balance, complemented by in-situ stake measurements for cross-validation, and integrates ground-based meteorological station records and reanalysis datasets to interpret the associated climatic contexts and underlying mechanisms. Based on these high-temporal-resolution daily surface mass balance datasets, ~~In this study, we applied time lapse photography at the Kangxiwa Glacier from 2019–2023, combined with in situ glaciological and meteorological measurements, to analyze the characteristics of daily accumulation ablation processes, interannual mass balance differences, and to investigate the impact of extreme heatwaves on high elevation glaciers in the eastern Pami~~this study aims to (1) characterize the contrasting seasonal mass balance patterns of the Kangxiwa Glacier in the eastern Pamir under varying climatic forcing regimes across the 2019/2020 to 2022/2023 balance years; (2) quantify the sensitivity of surface mass balance to the extreme 2022 summer heatwaves; and (3) identify the atmospheric circulation anomalies linked to the 2022 heatwaves using ERA5 reanalysis data, and further ~~elucidate~~explore regional glacier response.

2. Study region~~s~~

The study area is located near Muztagh Ata (7546 m a.s.l.) and Kongur Shan (7719 m a.s.l.) in the eastern Pamir, Central Asia (Fig. 1). This region hosts a total of 434 glaciers covering 1018 km², with a continental glacier regime characterized by cold and arid conditions (Shi & Liu, 2020). The climate of eastern Pamir is dominantly controlled by the westerly jet stream (Yao et al., 2012). Data from the Taxkorgan Meteorological Station (3091 m a.s.l., ~50 km south of Muztagh Ata) show a mean ~~summer~~ annual temperature ~~(June–August)~~ of ~~15.1~~3.7°C and annual precipitation of ~70 mm

duringover the period of 1960-2015 (Li et al., 2022; Lv et al., 2020).(1965–2023), concentrated between April and September.

Kangxiwa Glacier (38.28°N, 75.28°E) is a debris-free valley glacier on the western slope of Kongur Shan, extending from 5350 m to 4960 m a.s.l. with an area of 1.86 km² and length of ~3 km. This glacier was selected as the benchmark glacier for long-term measurements (Yao et al., 2022). Geodetic estimates indicate that the average mass balance of Kangxiwa Glacier was -0.13±0.99 m water equivalent (w.e.) and a near-balanced regional glacier mass state of surrounding glaciers(+0.13±0.10 m w.e.) in the whole eastern Pamir during 2000–2019 with +0.13±0.10 m water equivalent (w.e.) during 2000–2019 (Hugonnet et al., 2021), with moderate mass loss of -0.07±0.20 m w.e. during 2019–2022 (Falaschi et al., 2023) and a low area shrinkage rate of -0.7±0.5% decade^{-1} from 2000 to 2017 –(Li et al., 2022). For the Kangxiwa Glacier specifically, the average mass balance during 2000–2019 was −0.13 ± 0.99 m w.e. (Hugonnet et al., 2021).

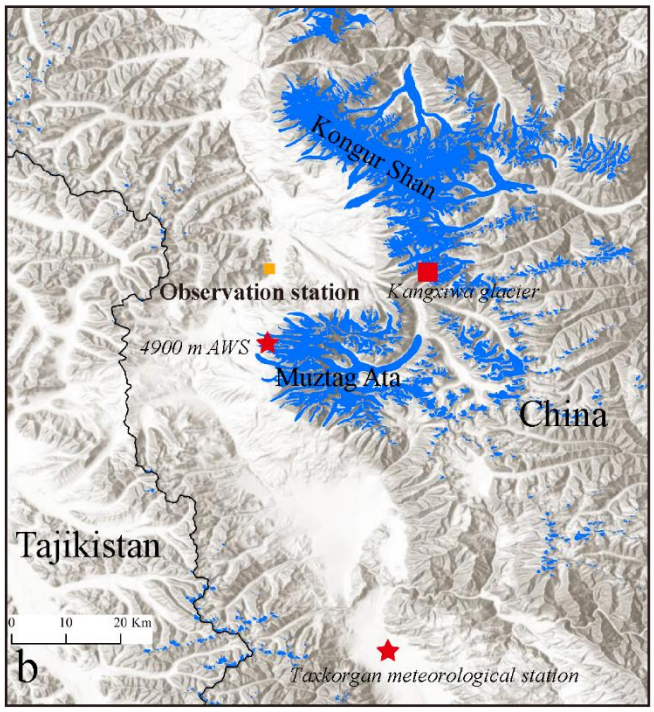
Kongur Shan
Observation station
Kangxiwa glacier
4900 m AWS
Muztag Ata
China
Tajikistan
0 10 20 Km
b
Taxkorgan meteorological station

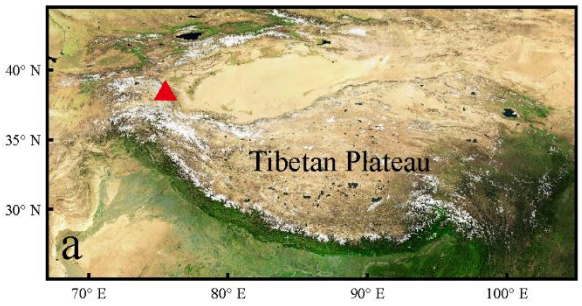
40° N
35° N
30° N
Tibetan Plateau
a
70° E
80° E
90° E
100° E

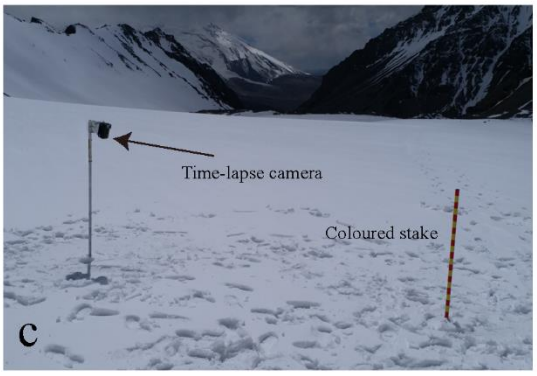
Time-lapse camera
Coloured stake
c

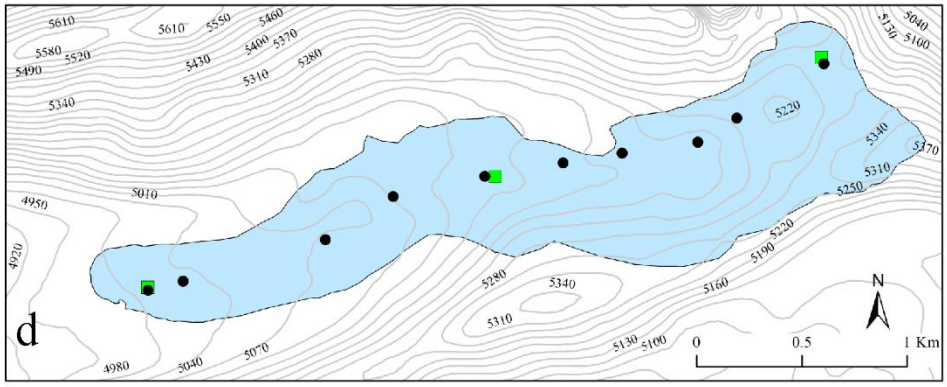
d
N
0 0.5 1 Km

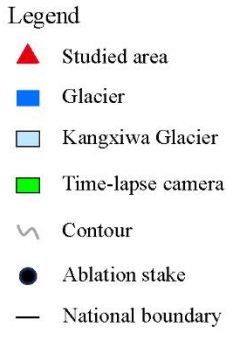
Legend
Studied area
Glacier
Kangxiwa Glacier
Time-lapse camera
Contour
Ablation stake
National boundary

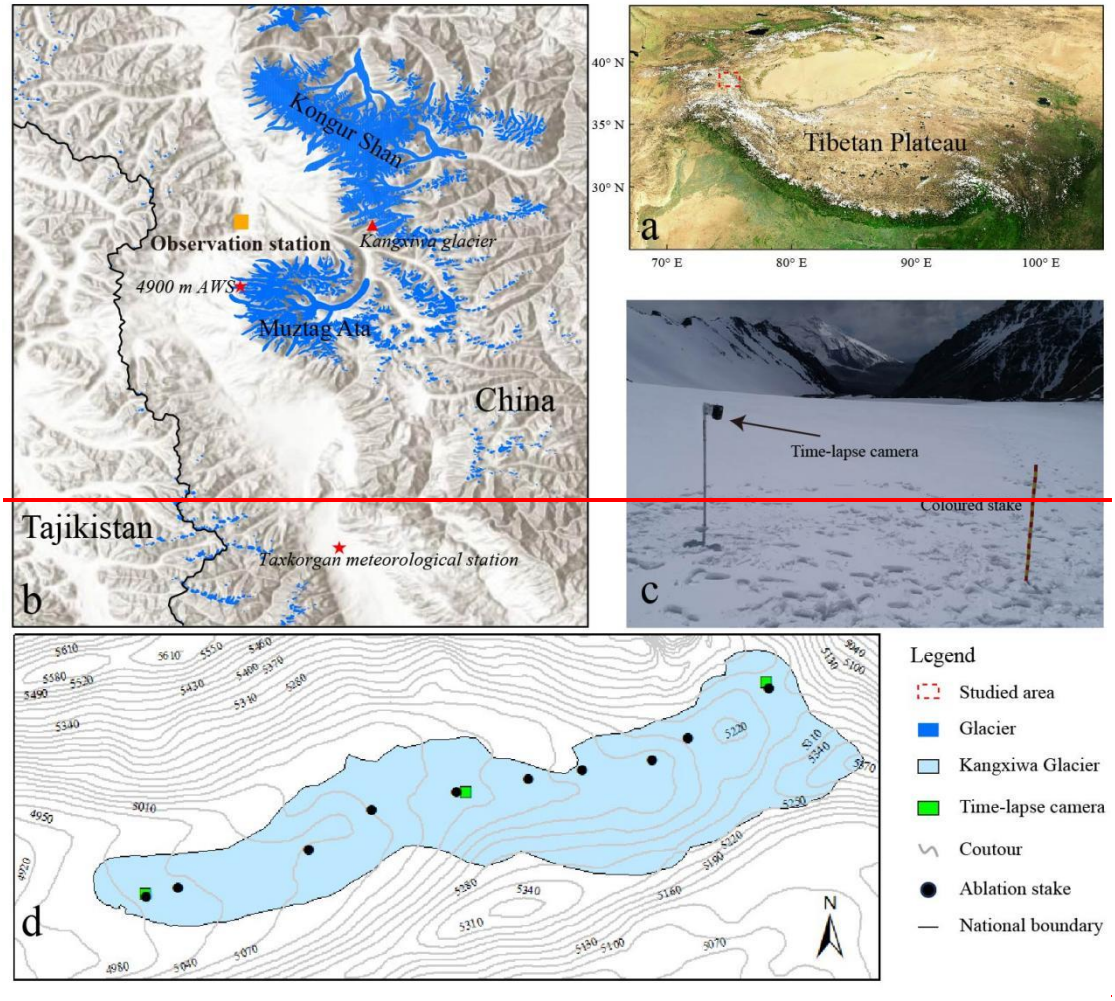

Figure 1. Study region and the distribution of in-situ measurements. (a) Location of the studied area in the eastern Pamir, central Asia; (b) The location of Kangxiwa Glacier (red ~~triangle~~square), Automatic Weather Station (AWS) at the elevation of 4900 m and Taxkorgan meteorologic station (red stars); the background is from World hillshade layer ~~was used as the background~~ (http://www.arcgis.com) and the glacier outline ~~of the glacier~~ was obtained from the Randolph ~~glacier~~ Glacier ~~inventory~~ Inventory (RGI 7.0~~; http://www.glims.org/RGI~~); (c) Photograph of the time-lapse camera and colour-coded stake on the Kangxiwa Glacier ~~(~~at 5300 m a.s.l.(~~,~~ 20 June, 2020); (d) Topographic map of the Kangxiwa Glacier showing the locations of three time-lapse camera monitoring systems and the ablation stakes~~/snow pits~~ for in-situ surface mass balance observations.

3. Data and Methods

3.1 Surface mass balance measurements by stakes and snow pits

Systematic glaciological observation of Kangxiwa Glacier has been conducted by the Muztagh Ata Station for Westerly Environment Observation and Research, Chinese Academy of Sciences (Fig. 1b). Ten ablation stakes were installed along the central flow line of the Kangxiwa Glacier to measure point-scale surface mass balance following standard glaciological methods (Cogley et al, 2011; Kaser et al, 2003~~Yu et al., 2013~~). ~~Field~~ In-situ measurements of stake exposure height, snow stratigraphy, and snow density were conducted at the onset~~start~~ (early June) and the end (late September) of each ablation season (Fig. 1d). Ice density was assumed to be 900 kg/m^3 (Huss, ~~et al.,~~ 2013). Seasonal (~~The~~ winter and~~,~~ summer) and annual point mass balance were ~~calculated~~ derived for~~during the period from~~ the 2019/2020 to 2022/2023 balance years. These annual and seasonal mass balances ~~during 2019–2023~~ serve~~s~~ as ground truth for validating the accuracy of daily surface mass balance retrieved from time-lapse camera observations ~~data~~ in this study.

3.2 Surface mass balance monitoring by time-lapse camera

3.2.1 Time-lapse camera monitoring systems

Three time-lapse camera systems were deployed at the glacier terminus (5005 m a.s.l.), mid-glacier (5137 m a.s.l.), and accumulation zone (5300 m a.s.l.) (Fig. 1d). The monitoring system adhered to methodologies established in prior research (Landmann et al., 2021; Cremona et al., 2023), integrating color-coded aluminum stakes and time-lapse cameras to quantify the stake ~~change~~ melt-out length~~in stakes' height~~. The aluminum stakes were marked at 5 cm intervals with alternating red and yellow bands (Fig. 1c~~-2a~~), installed vertically on the glacier surface and photographed hourly by fixed-position Forsafe H801 time-lapse cameras. The distance between each stake and its corresponding camera was approximately 6-10~~10~~ meters. Powered by 8 AA batteries and a solar panel, the cameras ensured continuous field operation. Featuring waterproof specifications, the camera captured images in JPEG format and stored them on a microSD card. In this study, cameras at 5137 m and 5300 m began operation on October 1, 2019 and the camera at 5005 m started on June 20, 2020. Seasonal maintenance included the replacements of stakes, microSD cards and batteries.

3.2.2 Changes of ~~stake hight~~ stake melt-out length

A semi-automatic procedure was developed to measure the ~~height of the coloured stake~~stake melt-out length, focusing on addressing the challenge of illumination variation in natural environments. The Hue-Saturation-Value (HSV) colour space was used for image processing because it separates luminance from colour information, unlike the standard RGB colour space where intensity and colour are intermingled. In the HSV method, H represents the colour type, such as red, yellow or blue; S refers to the purity of a colour, describing how much a pure colour is diluted with white light; and V represents the colour's brightness, ranging from black to white. These characteristics make

HSV particularly suitable for analysing and segmenting images captured under diverse lighting conditions (Ganesan et al., 2014; Hamuda et al., 2024; Yu et al., 2021).

Prior to image processing, photographs taken between 12:00 and 19:00 were selected to ensure optimal lighting, and blurry images taken during heavy snowfall were manually excluded. A fixed frame was then defined to encompass the stake, leveraging its stable position across consecutive shots (~~see~~ Fig. 2a). Stake contour detection relied on exploiting the difference in saturation values between the stake and the glacier surface (Fig. 2b). This involved applying a Gaussian filter to suppress high-frequency noise, followed by a morphological top-hat filter on the ~~S~~ S-channel of the HSV colour space to enhance differentiation between the stake and the background. The method proposed by Otsu~~'s method~~ (1979) was used for automatic thresholding during S-channel binarization, with the largest connected region selected as the stake in order to eliminate minor segmentation artefacts.

The pixel length of the stake (L_p), which is defined as the height of the minimum bounding rectangle (~~see~~ Fig. 2c), was converted to a real-world length in ~~centimeters~~centimetres (L) using a linear relationship (Fig. S1). This relationship was established through a comparative analysis of L_p and L in reference images. Reference images were manually selected to cover the full measurement range of L_p~~.~~ ~~.~~ For each reference image, L was manually calculated by incorporating the total number of visible ~~colored~~coloured bands (N), the pixel length of the bottom section (L_{pb}), and the pixel lengths of the two adjacent upper bands (L_{pa}), which were manually counted and measured, respectively. Figure S1 shows the significantly ~~strong~~ linear relationships between L and L_p of the reference images for each monitoring period at each monitoring site.

$$L=(N-1)\times 5+ L_{pb}\times 10/ L_{pa} \quad (1)$$

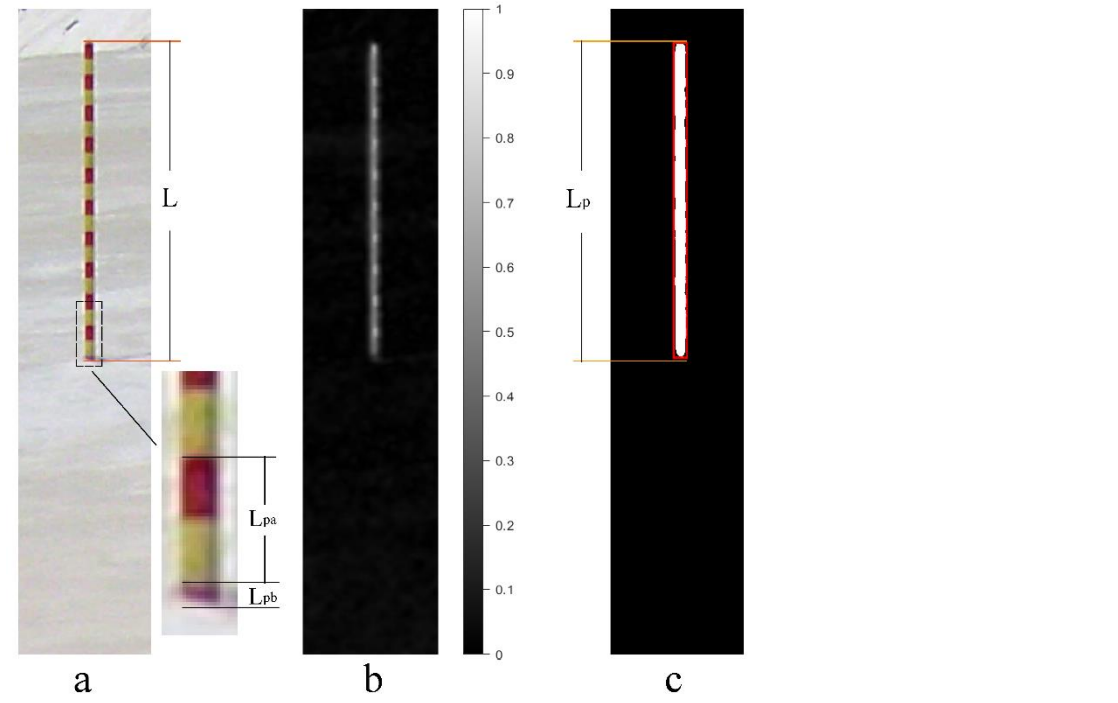

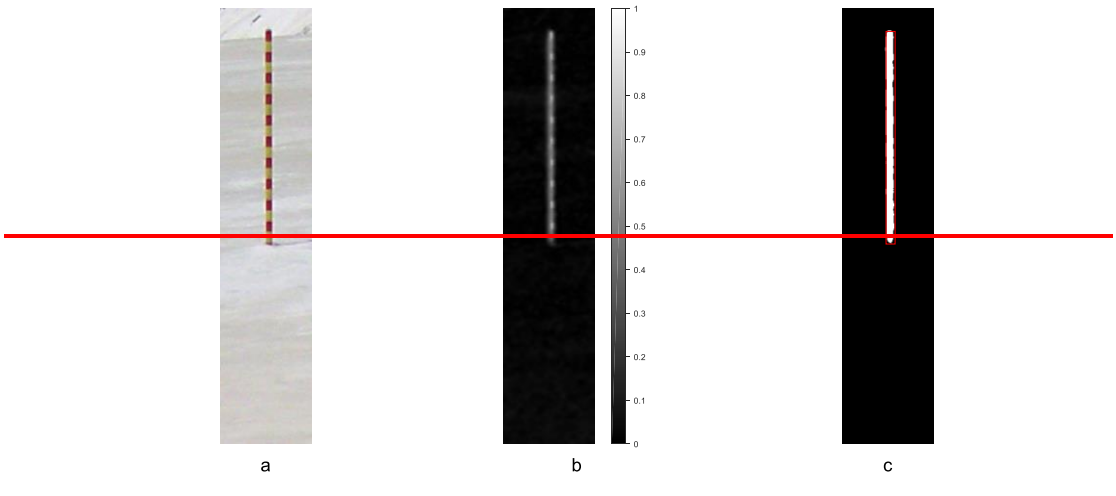

~~**Figure 2.** Illustration of image processing. (a) The original image with a frame; (b) the grayscale representation of the S channel; (c) the contour of the scale stake with the minimum bounding rectangle in red.~~

Figure 2. Illustration of image processing workflow. (a) ~~The o~~Original image with a frame and ~~. The bottom part of the stake is shown in a magnified view~~a zoomed inset of the ~~ablation~~ coloured stake bottom. (b) grayscale representation of the S channel from the HSV ~~color~~colour space~~the contour of the scale stake with the minimum bounding rectangle in red~~; (c) calibration stake contour with a red minimum bounding rectangle~~the grayscale representation of the S channel~~.

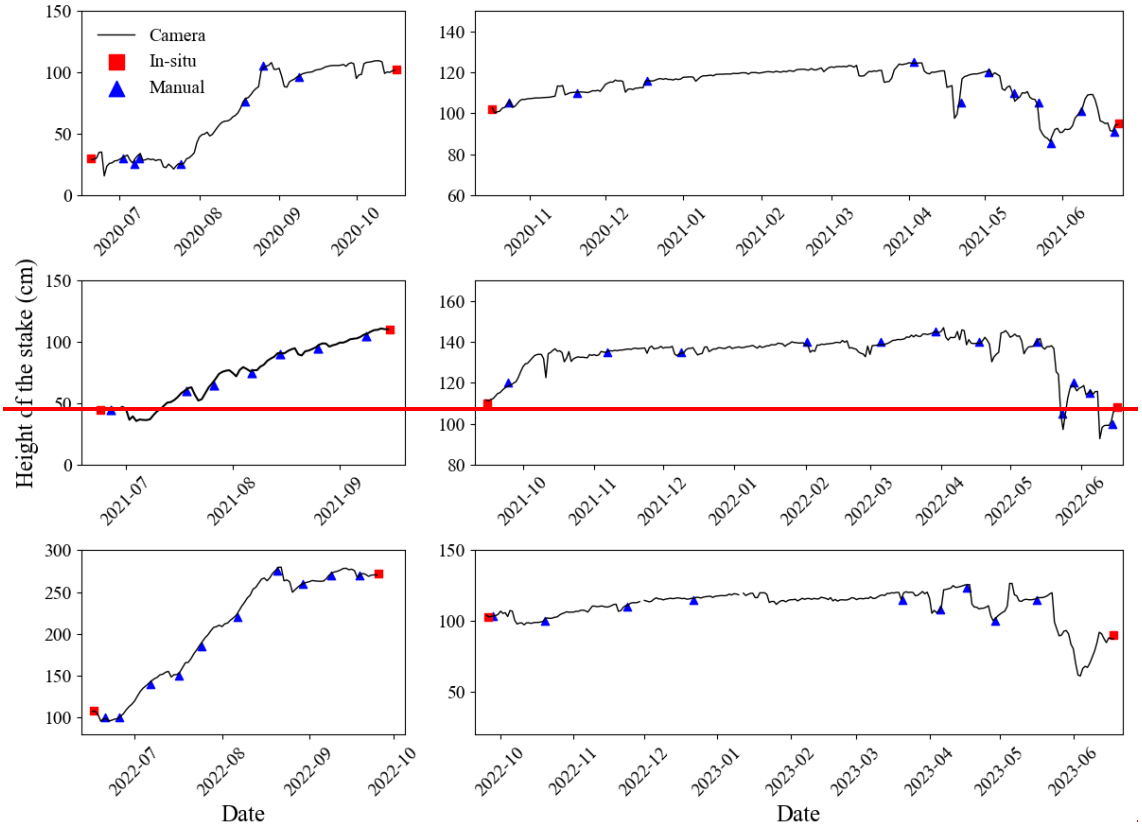

~~**Figure 3.** The performance of stake changes derived automatically from time-lapse cameras (black line), compared with in-situ observations (red square) and manual calculations (blue triangle) for a stake at the elevation of 5005 m asl. Noted that the camera monitoring systems were maintained in June and September in each year during the period from 2020 to 2023.~~

The performance of stake melt-out length~~stake changes~~ derived ~~automatically~~ from time-lapse cameras was validated by comparing with manually camera photo inspection and ~~in situ stake observations~~tape measurements during field campaigns (Fig. S2)~~and manually calculated results (Fig. 3)~~. During the image selection for manually inspection~~reading~~, the reference images were excluded to ensure the independence of the validation dataset. The semi-automated procedure demonstrated strong agreement with both methods, yielding a range of ~~agreement with both methods, with a mean difference of 0.30 cm~~ 3 cm to 2 cm across the validation samples.~~across 56 manual validation samples, and a range of 2.7 to 0.18 cm (mean 0.73 cm) for in situ readings.~~ These comparisons highlight the robustness of the time-lapse camera-based semi-automated workflow for quantifying stake melt-out length variations~~the monitoring stake hight changes by time lapse cameras, which has broader applications in studying surface mass balance dynamics at multiple elevations (Fig. 4)~~.

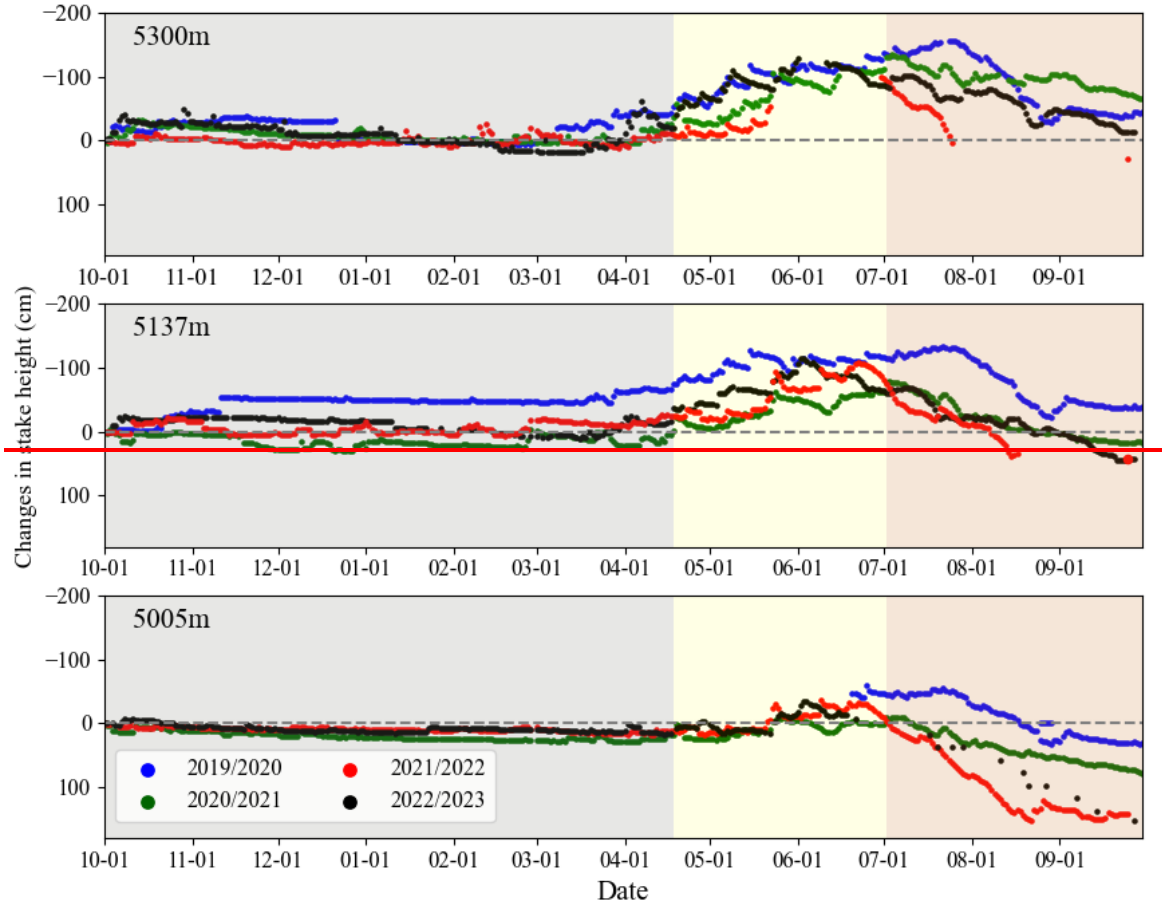

~~**Figure 4.** Changes of stake height at three elevations of the Kangxiwa Glacier during the hydrological years from 2019/2020 to 2022/2023.The relative change of stake height to the first day of each hydrologic year was set to 0 cm at the beginning of each hydrologic year.~~

3.2.3 Glacier mass balance ~~estimation~~ derived from ~~change in stake height~~stake melt-out length

The daily changes in the ~~height of the color-coded stakes~~stake melt-out length ~~at the~~recorded by three ~~points~~cameras ~~(Fig.1d)~~ were converted into changes in mass balance by multiplying by the corresponding density for ~~the~~ different surface conditions ~~(snow vs. bare ice)~~ through visual inspection of the photos manually (Fig. S3) ~~(Fig. S2)~~. For bare ice, a density of 900 kg/m³ was used. For snow surfaces, a mean snow density of ~~450~~ 405 kg/m³~~,~~, which was ~~was applied (~~the average density of snow pits measured at the three monitoring sites ~~in June~~ over the period 2020–2023~~,~~) was applied. To account for uncertainty ~~arising~~ from ~~variations in~~ snow density, ~~minimum and maximum~~two boundary values of ~~300~~ 286 kg/m³ ~~(lower part density of the snow pit at the 5005 m point at 23 June 2021)~~ and ~~600~~ 587 kg/m³ ~~(middle part density of the snow pit at the 5005 m point, 27 June 2024)~~, which were the minimum and maximum snow densities measured during the onset and later ablation season~~respectively~~, were incorporated into the analysis. ~~The mean daily mass balance values were calculated to fill data gaps which was caused by unexpected camera monitoring discontinuities. Since no camera monitoring was~~

~~conducted at 5005 m site from1 October 2019 to 20 June 2020, the daily average mass changes derived from in-situ measurements were used to fill the data gap.~~Limited data gaps were interpolated using adjacent measured values. The data gap at the 5005 m site from 1 October 2019 to 20 June 2020 was filled via daily mean mass balance value derived from the corresponding stake measurements (Fig. 3).

~~The mean differences of the 3 points are -71.764, -13.0 and -16.22 mm w.e., with standard deviations of 174.0192, 89.1137 and 134.0104 mm w.e. respectively, confirming the reliability of the camera-based approach. Overall, glacial mass balance changes calculated using the camera-based method are lower than those derived from field measurements. This is particularly notable during the 2022/2023 ablation season at the 5005 point, where the difference reached -409.02 mm w.e. – the largest discrepancy observed. This is likely because ice and firn were mixed on the glacier surface during this period; however, we identified the surface material as firn based on the images. This misidentification led to an underestimation of surface material density, which in turn resulted in an underestimation of surface mass loss.~~

Glacier-wide daily mass balance was then derived ~~via~~ by area~~a.~~ weighted ~~average~~ sum of point-scale mass balance estimates from the three cameras~~the three point values, with weights assigned by elevation-specific area proportions~~. A 30-m resolution SRTM DEM was employed to quantify the area distribution with its elevations. The cameras were deployed near the terminus, middle and upper region of Kangxiwa Glacier, allowing the entire glacier to be partitioned into three distinct zones centered approximately on each camera's installation site. These three zones ~~Digital elevation model (DEM) data (http://www.gscloud.cn/) with a resolution of 30 m × 30 m were used to partition different elevation ranges. Based on the contour lines at a 40 m interval (starting at 4960 m) and the mid-elevation between each pair of points, we determined the boundary elevation for every adjacent point pair. The three measurement points~~ corresponded to~~represented~~ the elevation ranges of 4960–5080 m (area weighting factor: 0.33)~~(weight: 0.33)~~, 5080–5200 m (area weighting factor: 0.38), ~~(weight: 0.38),~~ and 5200–5390 m (area weighting factor: 0.29) ~~(weight: 0.29)~~. ~~Gaps in camera data were filled using daily mean mass changes for the corresponding periods. For example, the net change in mass balance during July 26 to September 25, 2022 at the 5300 site was -87.61 mm w.e. (450 kg/m^3 multiplied by the net change in stake height), the daily average mass balance was 1.41 mm w.e.~~ Notably, each zone aligns with one camera deployment location and accounts for roughly one-third of Kangxiwa Glacier's total area. Kangxiwa Glacier features relatively flat topography (Fig. 1), and mass balance measurements from 10 ablation stakes further confirmed a linear elevation-dependent mass balance~~gradienFig.~~. These characteristics justified the extrapolation of glacier-wide mass balance from the limited set of point observations. Finally, the camera-derived mass balance estimates were validated against results obtained via traditional glaciological methods based on the 10 ablation stakes across the glacier.

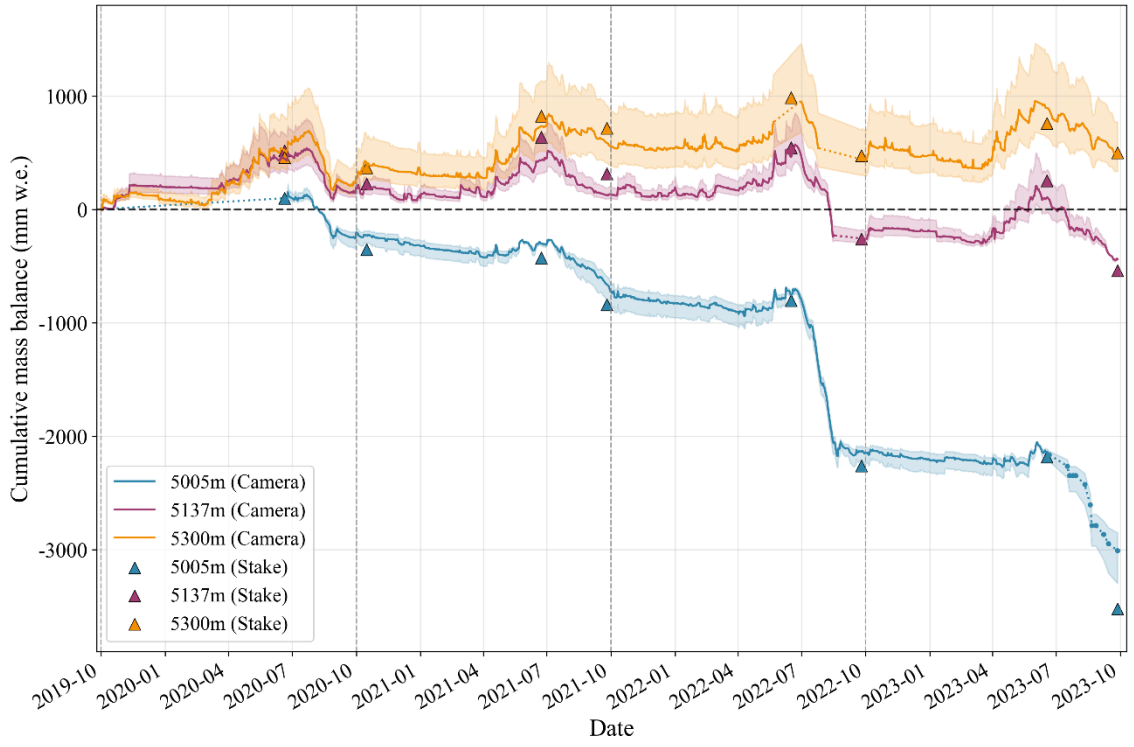

~~Notably, the 5005 m site was inactive from 1 October 2019 to 20 June 2020. During this period, daily average mass change of the in-situ measured values were used for glacier-wide calculations.~~

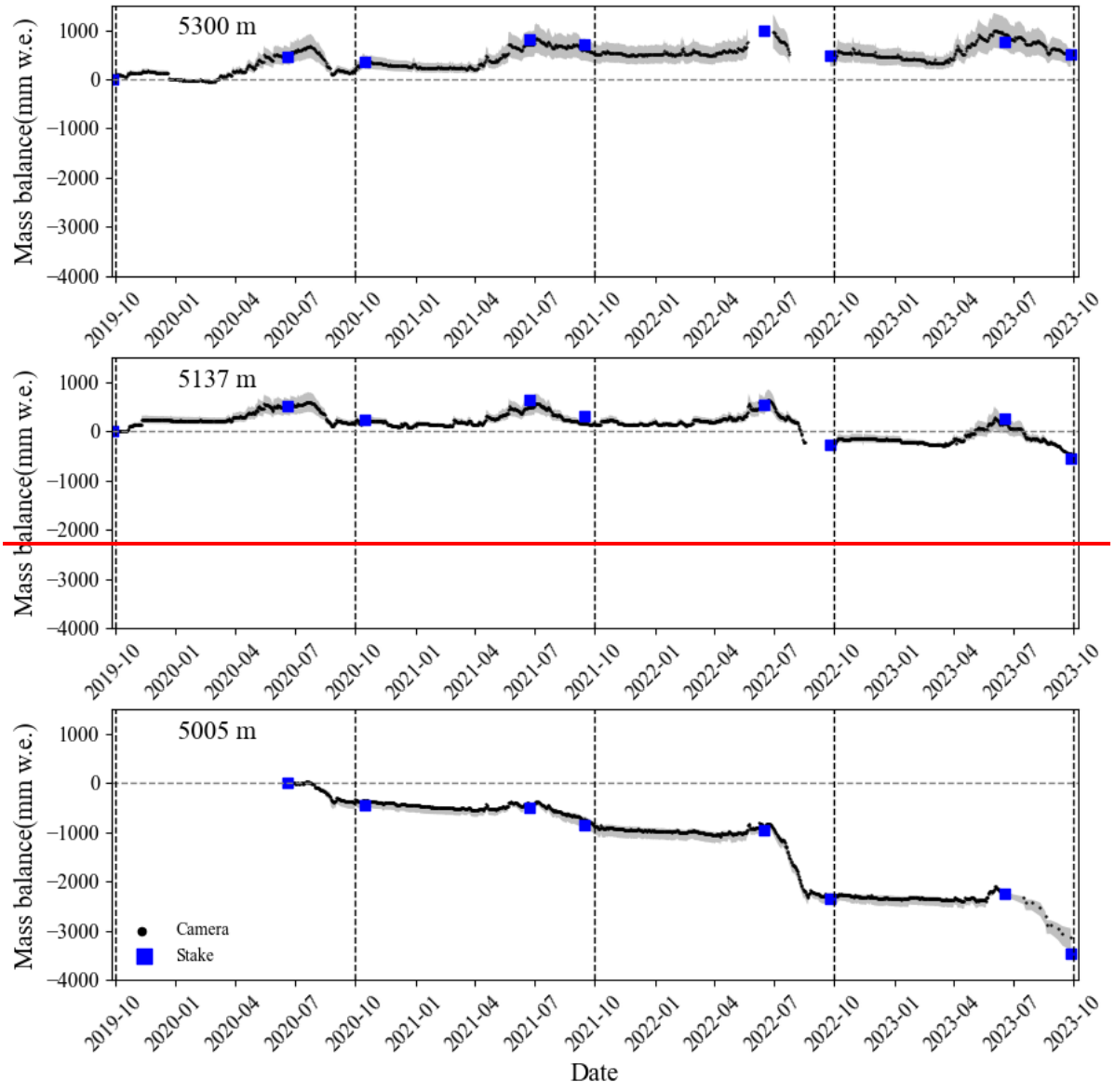

Figure ~~5~~3. Comparison of the accumulated mass balance estimated using time-lapse cameras (~~black~~ lines) and the glaciological methods (~~blue squares~~triangles) at the three locations (5005 m, 5137 m and 5300 m) on the Kangxiwa Glacier. The thin dotted lines denote gap-filled data.

3.3 Meteorological stations and the reanalysis data

A Caompbell automatic weather station (38.28°N, 75.04°E, 4900 m a.s.l.; AWS4900; Fig. 1b) was deployed on the western slope of Muztagh Ata in 2011 at a similar elevation to the Kangxiwa Glacier terminus. It continuously recorded half-hourly measurements of wind speed, wind direction, air temperature, relative humidity, atmospheric pressure,

incoming/outgoing shortwave and longwave radiation, and all-weather precipitation by T200B precipitation gauge (Zhu et al., 2018). This dataset was used to characterise the near-surface meteorological features of the study area over the past four years and identify extreme weather events. This provides a basis for explaining short-term abnormal changes in glacier mass balance. Data from the Taxkorgan Meteorological Station ~~(3091 m a.s.l.)~~, located approximately 50 km south of Muztagh Ata, ~~were~~ was used to ~~analyze~~analyse long-term climate change trends in the ~~East~~ east Pamir.

To investigate the possible climate mechanism on abnormal glacier mass loss, t~~T~~h~~e~~is study also employed the fifth generation of reanalysis data from the European Centre for Medium-Range Weather Forecasts (ERA5) with 2.5º horizontal resolution, which has been widely used in climate research (Hoffmann et al., 2019; Song et al., 2024) and glacier change analyses (Zhu et al., 2024b). By ~~analyzing~~analysing the spatial anomalies pattern of geopotential height, wind fields, and surface air temperature, we investigated the change of ~~how~~ large-scale atmospheric circulation and discussed its possible influences on extreme weather events and the subsequent responses of~~abnormal~~ glacier surface mass balance~~ablation~~.

4. Results

4.1 Performance of glacier mass balance estimation based on time-lapse camera observations

Figure 3 shows a comparison of the cumulative point mass balance estimates derived from the time-lapse cameras and the glaciological method at the three camera sites (5005 m, 5137 m and 5300 m) on the Kangxiwa Glacier during the period from 2019/2020 to 2022/2023 balance years. Figure 4a further presents the seasonal comparative performance of point-scale mass balance (winter and summer). Quantitative comparisons reveal that the mean seasonal mass balance differences between the two datasets at the three monitoring sits are −64, −13, and 2 mm w.e, with corresponding standard deviations of 193, 137 and 104 mm w.e., respectively. Over the entire observation period, the mean discrepancies between the two datasets across three points yield an overall mean of 26 ± -149 mm w.e.

At the glacier-wide scale (Fig. 4b), the camera-based seasonal mass balances exhibit a robust linear correlation with the stake-based counterparts (e.g., R^2 = 0.98), with almost all in-situ stake-based values falling well within the uncertainty bounds of the camera-based estimates. The mean discrepancy between the two datasets is 62 ± 54 mm w.e., indicating high consistency between the camera-based ~~approach~~method and the glaciological stake method. This robust agreement not only validates the reliability of time-lapse camera observations for quantifying glacier mass balance but also establishes a solid foundation for investigating temporal evolution characteristics of glacier-wide mass changes for the Kangxiwa Glacier.

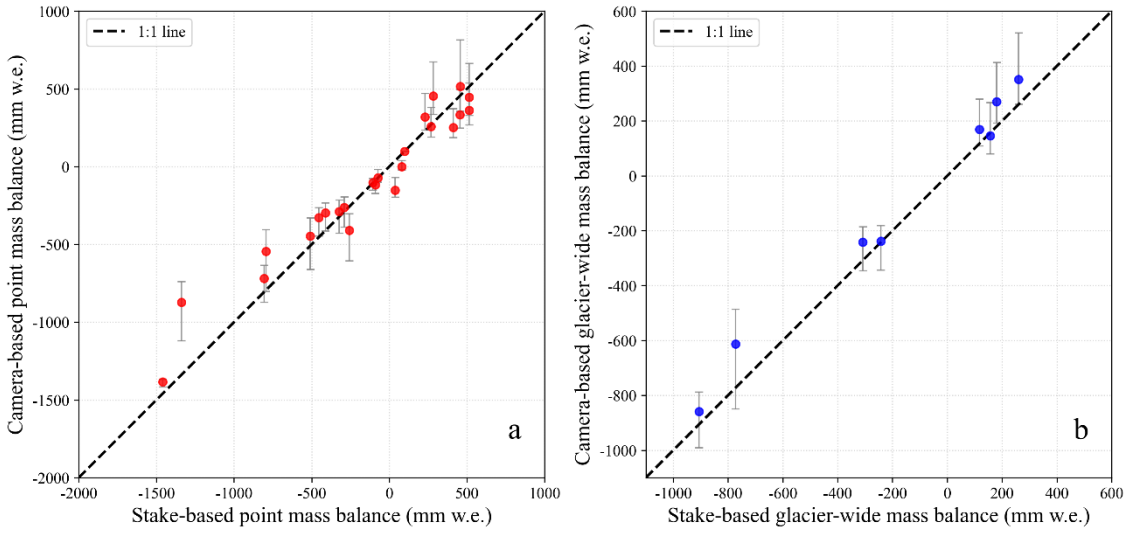

~~4.~~ **Figure 4** The comparison of point-scale mass balance (a) and glacier-wide mass balance (b) measured by using the stake method and the time-lapse photography on the Kangxiwa Glacier.

4.~~1~~ 2 Evolution of glacier surface mass balance during the 2019/2020-2022/2023 hydrological years

Figure ~~6~~ 5a compared the annual cumulative changes in the glacier-wide surface mass balance of the Kangxiwa Glacier during the 2019/2020–2022/2023 hydrological years, which can be broadly categorised into three phases: a balance period from October to mid-April, a snow accumulation period from mid-April to June/July, and an intense ablation period from June/July to September ~~(Figs. 6 and 7)~~. During the balance period, low temperatures and low precipitation resulted in limited changes in ~~stake height~~the stake melt-out length, with the cumulative mass balance fluctuating between ~~-80~~ 78 and ~~+185~~ 188 mm w.e. The slight surface mass loss observed during this period was ~~primarily~~ likely caused by sublimation or mechanical snow ~~erosion~~ drift driven by strong winter wind, as ~~which was~~ evidenced by the ~~abrupt~~ transition off~~from~~ snow-covered surfaces to exposed bare ice under cold winter conditions (Fig. ~~S2~~S3). During the accumulation period (mid-April to June/July), the glacier experienced different maximum snow accumulation across the entire glacier ranged from ~~270~~258 to ~~410~~445 mm w.e. ~~the glacier experienced substantial snow accumulation.~~ At an elevation of 5300 m asl, maximum snow depth reached 1.0-1.5 m (Fig. S3~~5~~) ~~(Fig. 4).~~, ~~while the average snow accumulation across the entire glacier ranged from a minimum of 270 to a maximum 410 mm w.e.~~ Notably, monthly accumulation peaks generally occurred in May (Fig. S4~~6~~). ~~(Fig. 7).~~

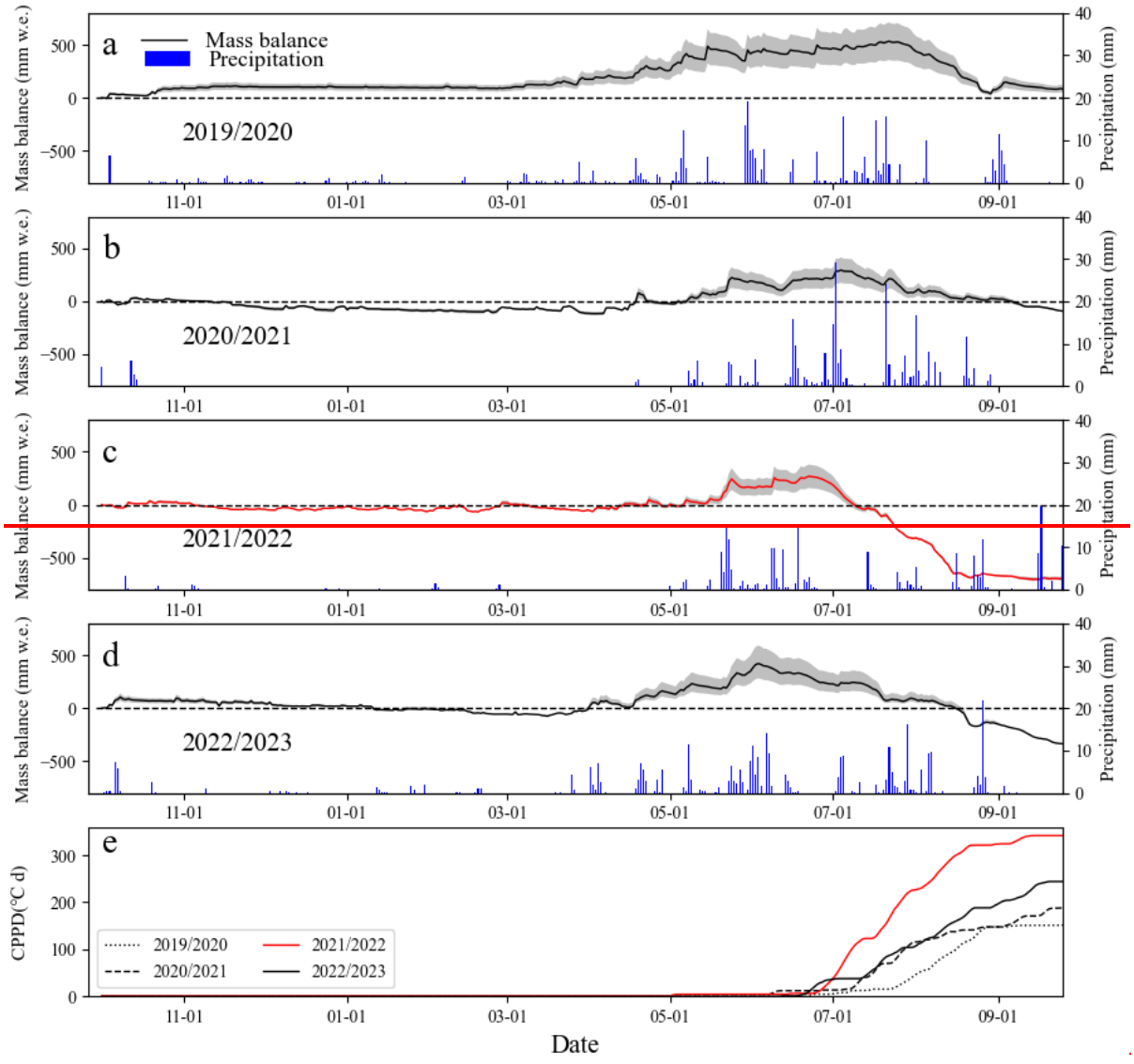

Figure 6. The contrasting evolution of the cumulative glacier-wide mass balance of the Kangxiwa Glacier with daily precipitation (a–d) and the accumulated positive degree recorded at AWS4900 (e) during the 2019/2020–2022/2023 hydrological years. The 2021/2022 hydrological year, which own significant mass loss, is highlighted in red.

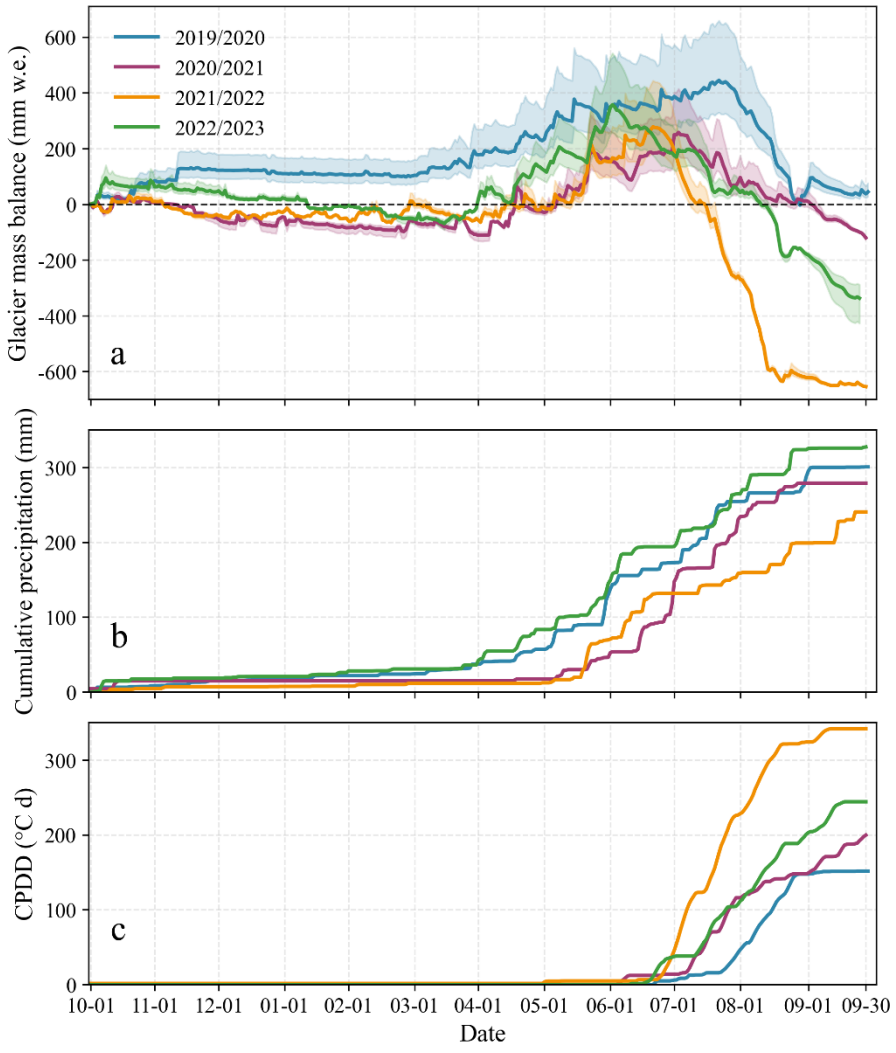

Figure 65. Cumulative glacier-wide mass balance of the Kangxiwa Glacier during the 2019/2020–2022/2023 hydrological years with the uncertainties by shaded area~~. Shaded area was error bands~~ (a). The ~~a~~accumulated precipitation (b) and the cumulated positive degree day recorded by the AWS4900 (c)~~ during the 2019/2020–2022/2023 hydrological years~~.

The phase of glacier mass loss is predominantly confined to the period from June/July to September, with significant interannual variability manifested in multiple key aspects. First, ~~(Figs. 6, 7)~~ the onset of surface mass loss—after the annual maximum ~~—since the maximum net accumulation—~~net accumulation is researched—exhibits substantial interannual differences:~~. This variability is evident in several aspects, beginning with the initiation of surface mass loss, which exhibits substantial interannual differences. T~~the earliest ~~summer commencement~~initiation was observed on around 2 June 2023, wh~~ereas~~ile~~ the latest occurred around ~~28~~ 22 July 2020. Concurrently, the ~~Glacier Loss Day (~~GLD~~)~~-defined as the date when

the net mass balance transitions to negative and all winter snow accumulation is depleted (Voordendag et al., 2023)-occurred on around 11 July 2022, approximately one month earlier than in other years (e.g., ~~~20 August 2020;~~ ~3 September 2021; ~26 August 2023). Notably, no GLD was recorded in the 2019/2020 hydrologic year, a phenomenon attributed to abundant winter-spring snow accumulation coupled with relatively low summer air temperature (Fig. 5b,c). ~~Voordendag et al. (2023) noted that the timing of GLD occurrence is primarily governed by the onset of glacier ablation, the accumulation prior to ablation, and the ablation rate from the start of ablation to the appearance of GLD. The absence of GLD in 2019/2020 was mainly attributed to the high spring and summer accumulation and the latest onset of ablation over the four-year observation period.~~The earliest GLD in the 2021/2022 hydrologic year was partly caused by the lowest precipitation in the accumulation season. Specifically, the AWS4900 shows that the cumulative precipitation for the 2021/2022 hydrologic year was only 131.84 mm until 11 July, while the corresponding values were 195.9 mm, 165.1 mm, and 218.7 mm for the 2019/2020, 2020/2021, and 2022/2023 hydrologic years, respectively.

~~The spring and early summer accumulation in 2021/2022 was lower than that in 2022/2023 and 2019/2020, yet slightly higher than that in 2020/2021. Although the onset of ablation was not the earliest, the ablation rate between the start of ablation and GLD occurrence was markedly higher than that in 2020/2021 and 2022/2023 (with values of 4.6, 5.7, and 12.9 mm w.e. for 2020/2021, 2021/2022, and 2022/2023, respectively). These factors led to the premature occurrence of GLD in 2022.~~ Beyond the timing of ablation onset~~In addition to the timing of initiation~~, the duration of glacier mass loss also exhibits marked interannual variability~~varies significantly from year to year~~. Specifically, it was approximately ~~30~~ 40 days in 2020 (from ~~28~~ 23 July to 30 August), 80 days in 2021 (11 July to 30 September), 58 days in 2022 (26 June to 22 August), and 120 days in 2023 (2 June to 30 September). Another interannual ~~dimension of~~ variability lies in the magnitude of annual surface mass loss, with values ~~with values~~ of -414, -334, -907 and -694 mm w.e. in the 2019/2020, 2020/2021, 2021/2022 and 2022/2023 hydrologic years, respectively.~~which ranges from -400 to -957 mm w.e~~. The most significant mass loss occurred in July–August 2022 (Fig. ~~7~~5), with the mass loss in July 2022 being four times greater than the three-year mean for the same period. AWS records indicate that interannual fluctuations in both ~~thermal~~ air temperature and precipitation ~~conditions~~ were the primary driver of significant differences in both the duration and intensity of surface mass loss during the 2019/2020–2022/2023 hydrological years (Fig. ~~6e~~5e). The exceptional mass loss in 2022, for instance, coincided with an anomalous summer of pronounced warming and aridity. This is evidenced ~~warming, as demonstrated~~ by the fact that accumulated positive degree days (CPDDs) at AWS4900 reached 341.7 ℃·day, which is 1.4-2.3 times higher than in the other three years, while total precipitation during July–August amounted to only ~~[XX]~~67.2 mm, approximately ~~[XX]~~50% lower than the average for the corresponding period across the other three years. ~~-~~

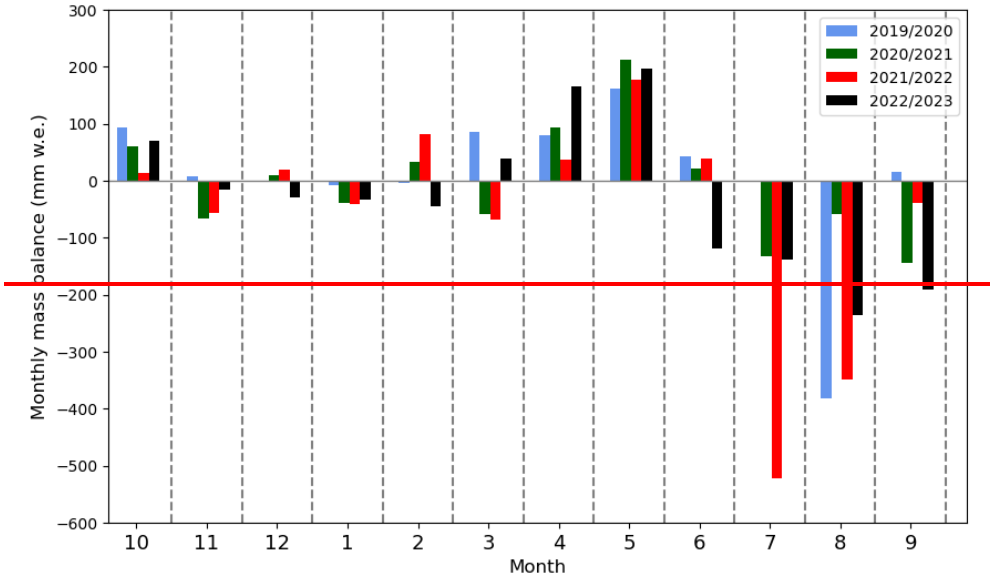

Figure 7. Comparison of monthly glacier mass balance of Kangixwa Glacier between four hydrological years of 2019/2020-2022/2023.

The annual mass balance of the Kangxiwa Glacier exhibited significant variability throughout the study period. A slight positive balance was recorded in the 2019/2020 hydrological year (+91 45 mm w.e.), followed by a weak negative balance in 2020/2021 year (-120 121 mm w.e.). This contrasts sharply with the substantial mass loss observed in the following two years: -707 64754 mm w.e. in 2021/2022 and -335 357336 7 mm w.e.in 2022/2023. Four-year observations revealed that the interannual accumulation differences of the Kangxiwa Glacier were limited to be ~260187 (258-445, mean 334±85)mm w.e., with the maximum accumulation of 537445 mm w.e. in the 2019/2020 hydrological year and the minimum of 278258 mm w.e. in the 2021/2022 hydrological year (Fig. 5). By contrast, annual mass balance fluctuations occurred between a slight positive balance of +45 mm w.e. in the 2019/2020 and a significant negative balance of -654 mm w.e. in 2021/2022, resulting in a divergence of 781669 mm w.e. A comparative analysis between the 2019/2020 and 2021/2022 reveals that less accumulation of 259167 mm w.e. in winter season, but more ablation of 522494 mm w.e. in summer season in 2021/2022. These results emphasize that interannual variability in the glacier mass balance of Kangxiwa Glacier was predominantly driven by the variability in mass loss during the ablation season. Over these four hydrologic years, the absolute values of net mass balance corresponding to the snow accumulation and ablation periods were determined to be 306±44 and 646±267 mm w.e., respectively, demonstrating that the mass change and the range of its variation in the ablation period were obviously greater than that in the accumulation period.

The mass changes during 2019/2020-2020/2021 are consistent with previous observations of limited mass loss in the Pamir region (Yao et al., 2012; Falaschi et al., 2023; Bhattacharya et al., 2021; Hugonnet et al., 2021). Meanwhile, linear altitudinal interpolation of two complementary datasets — camera-derived based point mass balances from data across

three elevations and stake-based measurement from 10 ablation stakes ~~— — —~~ enabled for the quantification~~estimation~~ of the mean equilibrium line altitude (ELA) ~~at ~ 5250~~ 5239 m a.s.l. over the study period. ~~This~~ The ELAs ~~, however,~~ displayed significant interannual fluctuations: ~~during 2021/2022,~~ the highest ELA surpassed the glacier summit during 2021/2022 balance year, whereas the lowest ELA ~~, at (~5091~~ 5079~5086 m a.s.l.)~~,~~ occurred in 2019/2020.

4.~~2~~ 3 Glacier response to the ~~unprecedented~~ heatwaves in the summer of 2022

Both ERA reanalysis data ~~, meteorological stations~~ and ~~,~~ ground-based meteorological station observations ~~ERA reanalysis data~~ revealed an unprecedented summer warming event in 2022 in the ~~East~~ east Pamir, with the most pronounced anomaly recorded ~~particularly~~ in July ~~2022~~ (Fig. 6 and Fig. ~~S3~~S5). The ERA5 temperature data confirmed that the corresponding grid point of the Kangxiwa Glacier in July 2022 was the highest recorded between 1981 and 2024 (Fig. 6a). The AWS4900 records evidenced that ~~T~~the average July temperature during 2012-2023 was 2.9°C, while it reached 6.2°C in July 2022, constituting a substantial positive temperature anomaly ~~representing a significant warm anomaly~~ (Fig. ~~5c~~6b). Additionally, ~~The~~ daily maximum temperature recorded at Taxkorgan station ~~in~~ during summer 2022 was significantly higher than the long-term mean for~~between~~ 1957 ~~and~~ 2023 (Fig. S5), with 61% of days in July exceeding the 90th percentile of historical temperatures and satisfying~~meeting~~ the criteria for an extreme heat event as defined by Lu et al. (2024). ~~Monthly air temperature in July 2022 was 3.8°C higher than the average over 2012-2023. The average July temperature during 2012-2023 was 2.9°C, while it reached 6.2°C in July 2022, representing a significant warm anomaly. Correspondingly, distinct differences were observed in the CPDD characteristics across different temperature intervals.The CPDD in the >8°C interval was significantly higher in 2022 than in other years of the study period.~~ Thisisese evidence ~~indicate~~indicatess that July 2022 was characterized by ~~a year with~~ significantly elevated ~~July~~ temperatures relative to historical baselines.

~~The ERA data also confirmed that the corresponding grid of the Kangxiwa Glacier in July 2022 was the highest recorded between 1980 and 2023.~~ This exceptional climatic event provides a unique opportunity to ~~analyze~~analyse how glaciers respond to extreme heatwaves in the eastern Pamir. ~~Based on AWS4900 records (Fig.1), three extreme heat events were identified between 26 June and 11 July, 18–30 July, and 5–17 August 2022 (Fig. 8).~~

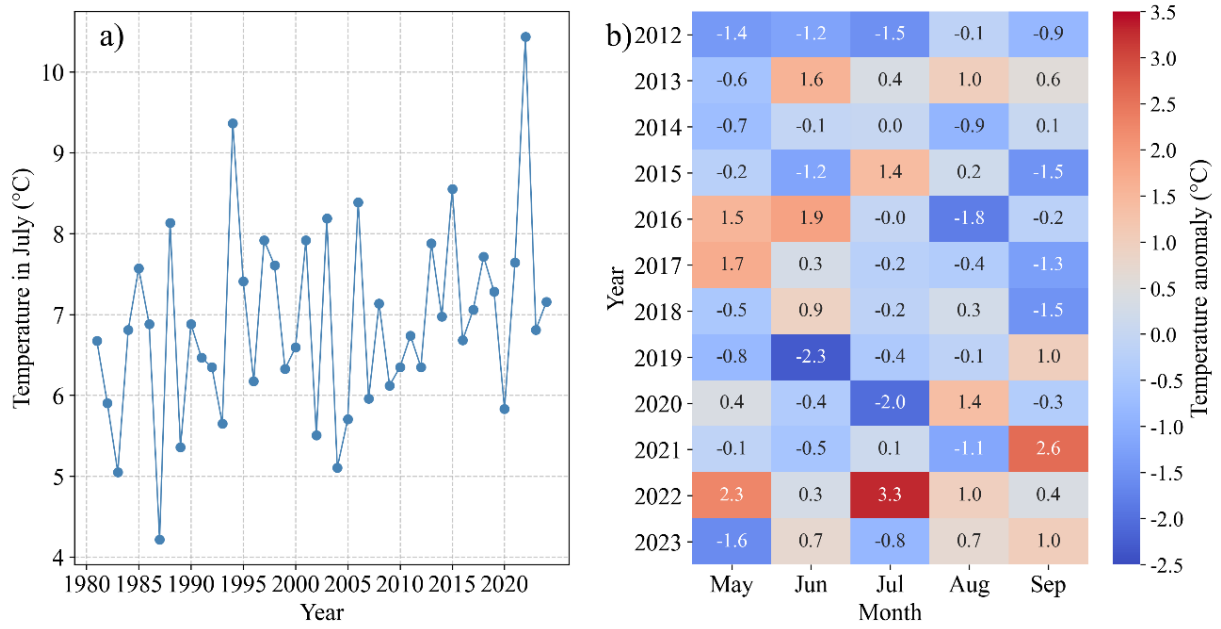

Figure 6. Variation of mean ERA air temperature in July at the corresponding ~~point~~ grid point of Kangxiwa Glacier during the period from 1981 to 2024 (a) and heatmap of monthly air temperature anomaly from May to September during 2012-2023 recorded by AWS4900 (b).

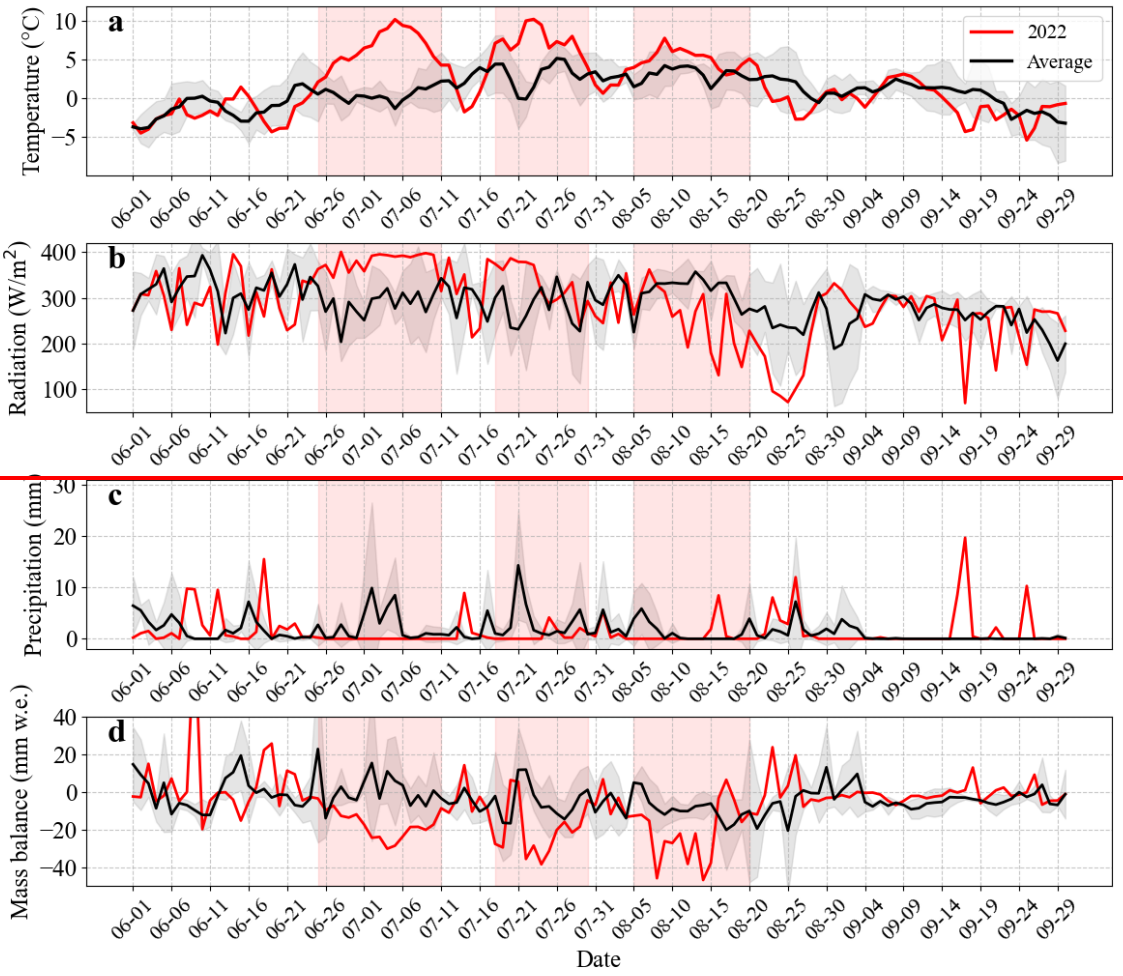
a
b
c
d
2022
Average
Temperature (°C)
Radiation (W/m²)
Precipitation (mm)
Mass balance (mm w.e.)
Date

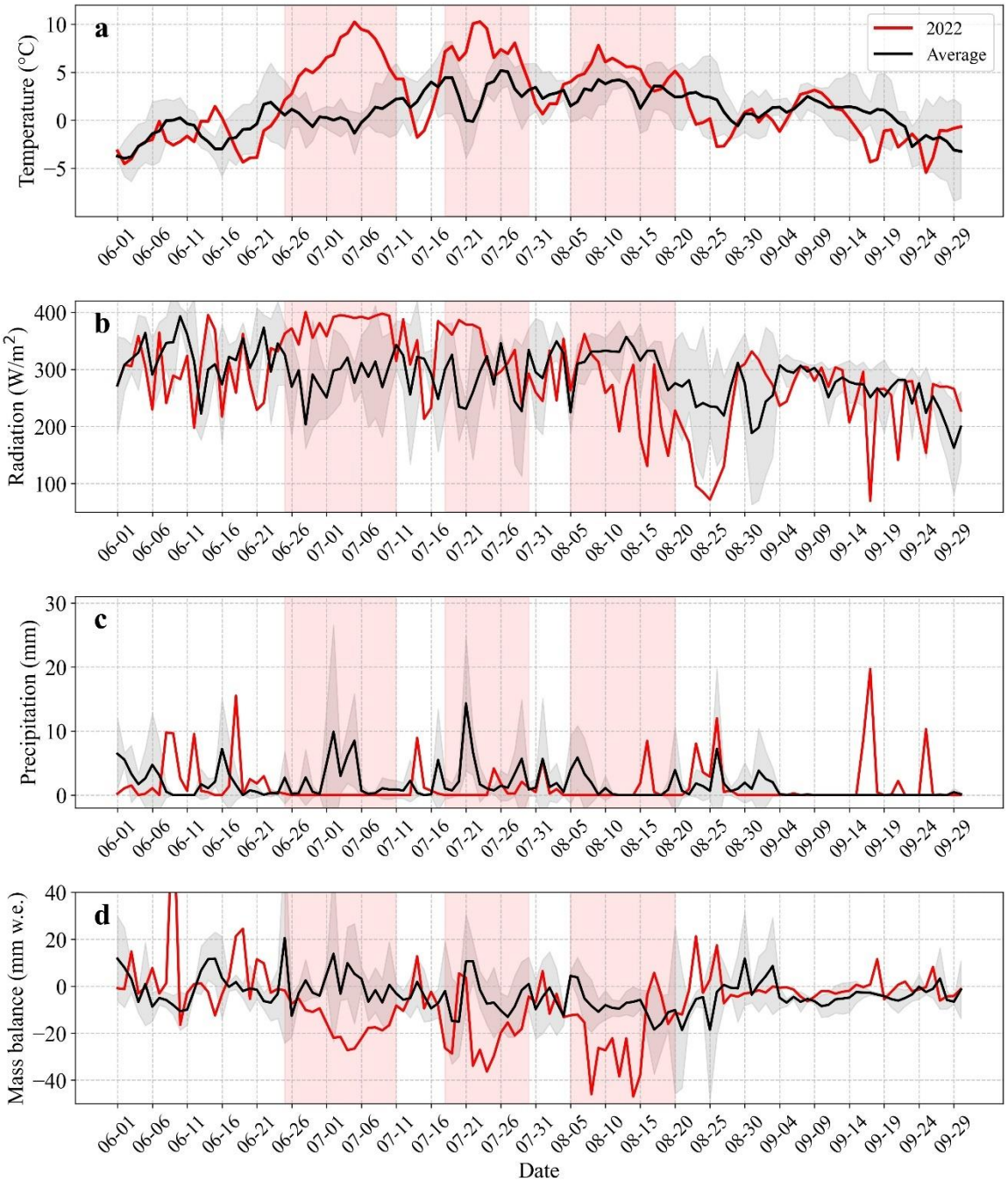

Figure ~~8~~7. Comparison of ~~(a)~~ daily air temperature(a), ~~(b)~~ daily incoming shortwave radiation(b), ~~(c)~~ daily precipitation(c) and ~~(d)~~ daily glacier-wide mass balance (d) at the Kangxiwa Glacier during the ablation season (June–September), showing the difference between 2022 and the other three years. The grey line shows the average for 2020, 2021 and 2023 with standardized variation (grey shaded area), while the red line shows the records for 2022. Light red rectangles highlight three heatwave events. The meteorological data was derived from the AWS4900.

Based on AWS4900 records ~~(Fig. 1)~~, three extreme heat events were identified between 26 June and 11 July, 18–30 July, and 5–17 August 2022 (Fig. ~~8~~7). During the first two heatwaves, daily temperatures were 6.2°C and 4.4°C higher than the three-year average, with a maximum anomaly of +10 °C on 5 July (Fig. ~~8a~~7a). Concurrently, daily incoming solar radiation exceeded the average by 90.6 W/m² (+31%) and 48.7 W/m² (+17%) (Fig.~~8~~7b), while total precipitation decreased by 40.4 mm (-100%) and 31.3 mm (-76%) ~~(Table 1)~~. These conditions, characterized by increased temperatures, reduced snow replenishment, and intensified solar radiation, drove anomalous mass loss (Figs. ~~5~~6, 7). The first extreme event induced a mean mass loss rate of ~~-17.9~~-16 mm w.e./day, whereas the three-year average for the same period exhibited a near-balanced state~~, with a mean value of only -0.20mm w.e./day~~. The second heatwave exacerbated mass loss to -~~20.0~~19 mm w.e./day, which is ~4 times the three-year mean (-~~1.0~~1 to -~~8.0~~7 mm w.e./day). This ~~unprecedented~~ significant ablation accelerated the depletion of spring-accumulated snow (Fig. ~~9~~8) and thus contributed to the advance of the ~~Glacier Loss Day~~GLD by one month (Fig. ~~5~~6).

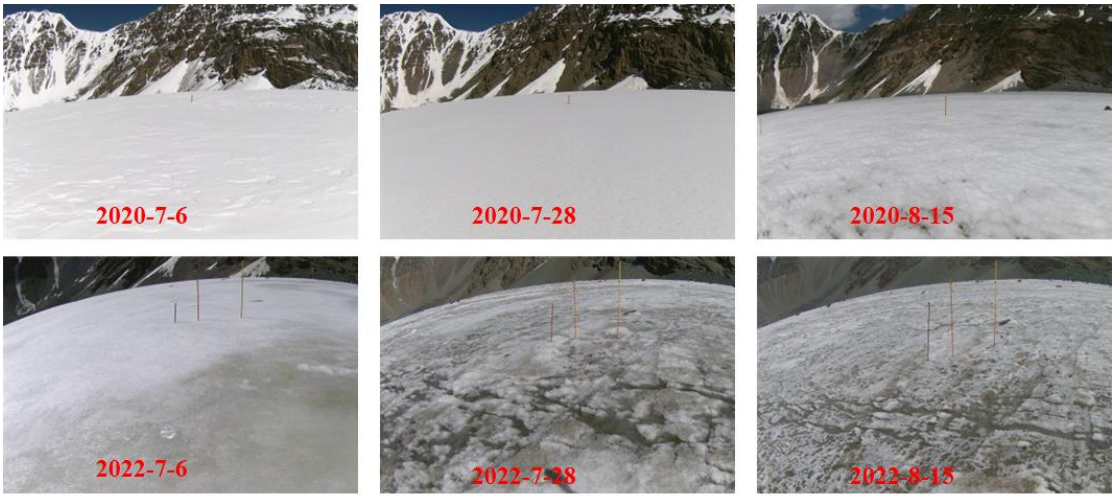

Figure ~~9~~8. Contrasting glacier surface conditions at the elevation of 5005 m between July–August 2020 and 2022.

The weather conditions during the August heatwave and the corresponding glacier response ~~of glacier~~ were obviously different from those during the two July heatwaves. The warming magnitude ~~of warming~~ in the August heatwave was only 2.5 ~~°C~~℃ higher than the corresponding temperature average of the other three years. The reduced shortwave radiation of 54.9 W/m² (-17.1%) and the increased longwave radiation of 26.1 W/m² (+10.2%) indicate the increased cloud cover over the eastern Pamir during this period (Liu et al., 2021). There was no significant change in precipitation ~~(Table 1)~~. The August heatwave was therefore characterized by ~~the relative~~moderate warming and cloudy conditions. In contrast, the magnitude of mass loss during the August heatwave was even more intensive~~greater~~ than those during the two July

heatwaves (Fig. 78b). Mass loss intensity increased to be 23.3 mm w.e./day during the August heatwave, which is 15.616 mm w.e./day higher than the mean value for the corresponding periods of the other three years.

Glacier surface melting is critically linked to the energy supply and the surface conditions. The precipitation phrase may greatly influence the snow accumulation and the surface albedo condition (Jouberton et al., 2022). Seasonal snowfall and rainfall amount at each camera-monitored site for each hydrological year were estimated using the method proposed by Ding et al. (2014), combined with meteorological data from AWS4900 and the Muztagh Ata observation station (3650 m a.s.l.). Snowfall accounted for 94% of total precipitation at the glacier terminus (5050 m a.s.l.), 96% at the mid-glacier site (5137 m a.s.l.), and 99% at the upper-glacier site (5300 m a.s.l.) in the warmest 2022. The scarcity of rainfall in summer season across the glacierized area indicates that precipitation phase transitions likely played a limited role in modulating the surface energy–mass balance. At the 5005 m site, the number of bare ice days from June to September 2022 reached 42 in 2021/2022, compared to 4, 23, and 13 days for the 2019/2020, 2020/2021, and 2022/2023 hydrologic years respectively. This marked increase in bare ice days enhanceds glacier surface energy absorption, which partly explained the substantial mass loss in the summer of 2022. Given the moderate temperature anomaly and reduced shortwave radiation during the August heatwave, the intensive mass loss could be primarily attributed to the exceptionally low surface albedo of exposed ice (Fig. 8), which amplified solar radiation absorption and subsequent melt processes (Mölg et al., 2014).

Givern Given the limited magnitude of warming and the reduced atmospheric shortwave radiations, this discrepancy could partly be attributed to the lowest surface albedo of exposed dirty ice (Fig. 9), enhancing solar radiation absorption for melting (Mölg et al., 2014).

Table 1 Daily anomalies of meteorological variables and mass balance during three heatwave periods in 2022 relative to the corresponding 2020–2021–2023 average.

Phase	Temperature (oC)	Shortwave Radiation (W/m2)	Precipitation (mm)	Longwave radiation (W/m2)	Mass balance (mm w.e/day)
I (6.26-7.11)	6.3	90.6	-2.5	-11.2	-17.7
II (7.18-7.30)	4.4	48.7	-2.4	-10.9	-15.0
III (8.5-8.17)	2.5	-54.9	-0.4	26.1	-15.6

The relationships between the monthly mass balance and the corresponding cumulative positive temperatures and precipitation further confirm the nonlinear responses of the glacier mass balance and the importance of surface conditions

(Fig. 10). In months with similar positive temperatures (e.g., August 2020, July 2021, August 2022 and August 2023), the magnitude of glacier mass loss varied significantly (-130 to -380 mm w.e.), whereas precipitation varied only within 100 mm. This indicates that differences in precipitation alone cannot explain these discrepancies. Similar to the August 2022 extreme loss, glacier surface conditions (e.g., albedo) at different periods may play a critical role in modulating the energy balance. The timing and intensity of heatwaves have a differential impact on glacier mass loss, which is mediated by snow/ice albedo feedback mechanisms. The relationships between the monthly mass balance and the corresponding cumulative positive temperatures and precipitation further confirm the nonlinear responses of the glacier mass balance and the importance of surface conditions (Fig. 10).

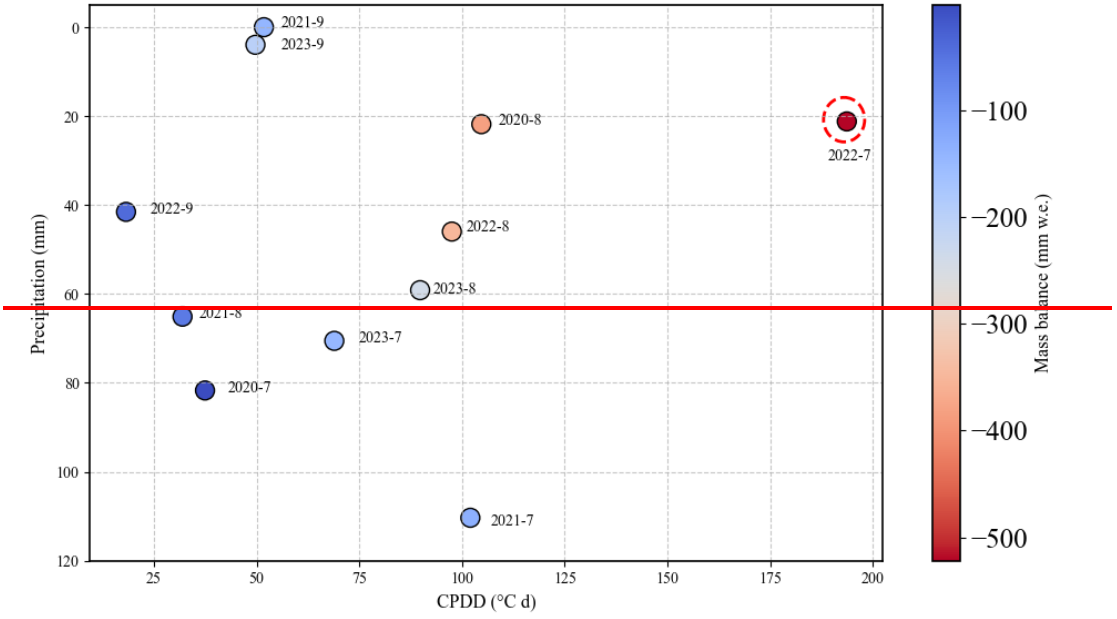

Figure 10. Relationships between monthly glacier mass balance, cumulative positive degree-days (CPDDs), and monthly precipitation during the 2020–2023 ablation seasons. The anomalous negative mass loss in July 2022 is highlighted by a red circle.

5. Discussions

5.1 Mass balance characteristics in the ~~East~~ eastern Pamir

~~Unlike the traditional seasonal or annual glacier mass balance observations (Zhu et al., 2018; Xu et al., 2024), this study presents the four-year records of daily-averaged glacier mass balance for a benchmark glacier in the East Pamir. Based on this dataset, it is evident that the accumulation in April–May is the primary determinant of annual accumulation magnitude. Barandum et al. (2018) found that glaciers in the West Pamir region that initiate received snow accumulation at the start of the hydrologic year receive over 1 m w.e. of snow accumulation during the winter season. These different accumulation patterns are linked to divergent precipitation seasonality between the East and West Pamirs, driving the formation of distinct mass accumulation types (Maussion et al., 20122014). Published geodetic estimates reveal striking west-east disparities in glacier mass balance since 2000, with a mean mass loss of −0.26 m w.e. a^{-1} in the Western Pamir but a near-balanced state (−0.02 m w.e. a^{-1}) in the Eastern Pamir (Bolch et al., 2019). Four-year observations revealed that the interannual accumulation differences of the Kangxiwa Glacier were limited to be ~260 mm w.e., with the maximum accumulation of 537 mm w.e. in the 2019/2020 hydrological year and the minimum of 278 mm w.e. in the 2021/2022 hydrological year (Fig. 6). By contrast, annual mass balance fluctuations occurred between a slight positive balance of +79 mm w.e. in the 2019/2020 and a significant negative balance of −702 mm w.e. in 2021/2022, resulting in a divergence of 781 mm. A comparative analysis between the 2019/2020 and 2021/2022 reveals that accumulation in 2021/2022.variability accounts for ~33% of the total mass balance difference, while differences in summer ablation contribute ~67%.. These results emphasize that interannual variability in the glacier mass balance in the eastern Pamir was predominantly driven by the variability in mass loss during the ablation season.~~

~~As illustrated in Figures 6 and 7, the mass loss in 2019/2020 was concentrated in August (−400 mm), following a period of high accumulation (+537 mm). In contrast, the 2022 mass balance process featured low spring accumulation and extremely strong summer ablation driven by heatwaves in July and August. While the ablation periods in 2021 and 2023 were significantly longer than in other years, the average summer ablation intensity was moderate. Unlike the stable mass accumulation observed in June across the other three years, the Kangxiwa Glacier experienced early ablation (−100 mm w.e.) in June 2023, followed by the highest ablation in September over the four-year period. Cumulative mass loss from June onward reached −880 mm w.e. in 2023, which was slightly less than the maximum loss in 2022. These divergent patterns of mass balance evolution not only underscore the complexity of glacier responses to climate change in this region and highlight the critical importance of continuous, high-time-resolution monitoring of glacier surface - mass changes using cameras.~~

Glaciers in the Muztagh Ata have been in a near-equilibrium state~~balance or less mass loss~~ since at least the 1970s (Kääb et al., 2015; Bolch et al., 2017, 2019a; Brun et al., 2017). Based on the high-resolution Pléiades ~~stereo~~stereo -images, Falaschi et al (2023) ~~analysis~~ analysess the annual and seasonal glacier mass balance in Muztagh Ata and address that the mean mass loss of 2020, 2021 and 2022 was -0.19±0.14 m w.e., +0.15±0.27 m w.e, ~~+~~ -0.17±0.22 m w.e. Our ~~ground~~

measurements at the Kangxiwa Glacier in the Muztagh Ata region~~s~~ at the 2019/2020 and 2020/2021 hydrological year are consistent with the previous knowledge of near-equilibrium~~less mass loss~~ in this region (Yao et al., 2012; Falaschi et al., 2023; Bhattacharya et al., 2021; Hugonnet et al., 2021). However, the mass balance in 2021/2022 and 2022/2023 hydrological years displayed the significant mass loss. In particular, the mass loss in 2022 was the most negative and agrees well with the reported unprecedented mass loss of the Urumqi No.1 Glacier in the eastern Tien Shan (Xu et al., 2024) and the notable mass loss in the European Alps (Berthier et al., 2023; Cremona et al., 2023; Voordendag et al., 2023). Similar to the Swiss glaciers, the equilibrium line altitude of the Kangxiwa Glacier rose above the glacier summit~~s~~ in 2022 due to heatwaves. Extremely high air temperatures covered Eurasia and North America, with long-lasting extreme heat events affecting China (Lu et al., 2023). During the summer of 2022, three heatwaves within a 40-day period caused a mass loss equivalent to over 90% of the total ablation losses for the season, demonstrating the pivotal role of heatwaves in driving local glacier ablation in this region.~~.~~ Similar regional heatwaves around the world (~~Oliver et al., 2018;~~ Colucci et al., 2017; Perkins-Kirkpatrick and Lewis~~et al.,~~ 2020; Zhang et al., 2025) pose substantial threat to mountain glaciers. Such significant mass loss by short-time heatwaves could influence the long-term ~~dynamics~~ changes of glacier ablation.

We further compared the published annual mass balance from the glaciers including Zulmart Glacier (Glacier No. 139), Glacier No. 457, and Abramov Glacier in Pamir and Tic~~a~~n S~~s~~han (WGMS, 2024~~4~~5). Similar to the Kangxiwa Glacier, the Zulmart Glacier in the Pamir, which is about 200 km northwestern from Kangxiwa Glacier, also exhibited the most negative mass balance in 2022, which is likely attributed to the same impact of extreme high temperatures in July. In contrast, neither the Abramov Glacier nor the No. 457 Glacier showed similar patterns. These contrasting mass loss patterns are likely modulated by divergent climatic regimes and topographic conditions, which influence mass change patterns and climatic sensitivities across the Pamir (Brun et al., 2019; Wang et al., 2019).

Based on our daily mass balance dataset, it is evident that the accumulation in April–May is the primary determinant of annual accumulation magnitude in east Pamir. Barandum et al. (2018) found that glaciers in the west Pamir region received snow accumulation at the start of the hydrologic year receive over 1 m w.e. of snow accumulation during the winter season. These different accumulation patterns are linked to divergent precipitation seasonality between the east and west Pamirs, driving the formation of distinct mass accumulation types (Maussion et al., 2014). Published geodetic estimates reveal striking west-east disparities in glacier mass balance since 2000, with a mean mass loss of -0.26 m w.e. a^{-1} in the Western Pamir but a near-balanced state (−0.02 m w.e. a^{-1}) in the eastern Pamir (Bolch et al., 2019).

Furthermore, variations in the timing of heatwave occurrence and their combination with seasonal distribution of precipitation can also contribute to substantial disparities in the response of glacier surface mass balance to climatic conditions. As illustrated in Figures 5, the mass loss in 2019/2020 was concentrated in August (-346 mm), following a period of high accumulation (+445 mm). In contrast, the 2022 mass balance process featured low spring accumulation and extremely strong summer ablation driven by heatwaves in July and August. While the ablation periods in 2021 and 2023 were significantly longer than in other years, the average summer ablation intensity was moderate. Unlike the stable mass accumulation observed in June across the other three years, the Kangxiwa Glacier experienced early ablation (-107 mm w.e.)

in June 2023, followed by the highest ablation in September over the four-year period. Cumulative mass loss from June onward reached -628 mm w.e. in 2023, which was slightly less than the maximum loss in 2022. These divergent patterns of mass balance evolution not only underscore the complexity of glacier responses to climate change in this region but also highlight the critical importance of continuous, high-temporal-resolution monitoring of glacier surface mass changes to inform future model-based explanations ~~via camera-based observations~~ (Barandun and Pohl, 2023).

5.2 The anomalous circulations in July 2022 and its influence on glacier balance

The extraordinary mass loss of the Kangxiwa Glacier in the eastern Pamir and Urumqi Glacier No. 1 in the ~~Eastern~~ eastern Tien Shan in 2022 (Xu et al., 2024) suggests that heatwaves may affect glacier conditions in the region on a wider scale. Analysis using ERA reanalysis data indicates that ~~the center of~~ the July heatwave event was mainly located on the Pamir Plateau (Fig. ~~11a~~9a). The overall impact of the 2022 heatwave was felt in the western Kunlun Mountains and the Pamir Plateau — regions where glaciers were previously considered in equilibrium or having a positive glacier mass balance~~stable or in positive equilibrium~~ (Brun et al., 2017; Kääb et al., 2015; Hugonnet et al., 2021).

We ~~analyzed~~analysed anomalies in temperature, solar radiation, cloud cover, geopotential height and wind fields at 200 hPa during July 2022, compared to the climatological average from ~~1970~~ 1991 to 202~~0~~2, to investigate the anomalous large-scale atmospheric circulations linked to the 2022 July mass balance anomaly in this study area. Anomalously high temperatures of over 4°C were observed across the Pamir Plateau and the western Kunlun Mountains. This suggests that other glaciers in the region may also have experienced significant mass loss during the summer of 2022. Latest research in the Northwestern Pamirs found that enhanced glacier mass loss was linked to the 2022 July heatwave (Jouberton et al., 2025). Numerous studies have linked heatwaves and high-temperature events to anticyclonic systems (Deng et al., 2023; Jiang et al., 2023; Song et al., 2024). Figure ~~11b~~ 9b shows that an upper-level anticyclonic anomaly developed over the northwestern flank of the Tibetan Plateau at 200 hPa. Under these circulation patterns, strong easterly wind anomalies occur on the southern side of the anticyclonic anomaly, reducing the westerly wind at 30–40°N. A decrease in westerly winds means less atmospheric water is delivered to the Pamir, resulting in reduced precipitation and cloud cover ~~(see Table 1)~~. Abnormal anticyclonic circulation can suppress convection and cause strong subsidence, resulting in reduced cloud cover (Figure ~~11d~~9d). The decrease in cloud cover, in turn, leads to increased incoming shortwave radiation. ~~Both Table 1 and ERA5 data (~~Figure ~~11e~~9c~~)~~ indicate anomalously high shortwave radiation during the July 2022 heatwave events. For example, AWS4900 records showed that ~~Table 1 shows that~~ shortwave incoming radiation exceeded the average for 2020–2021–2023 by 90.6 W/m² (+31%) and 48.7 W/m² (+17%) during the two heatwave events. This enhanced solar radiation further amplified the heatwave. ~~For example, Table 1 shows that the shortwave incoming radiation during the two heatwaves exceeded the average for 2020–2021–2023 by 90.6 W/m² (+31%) and 48.7 W/m² (+17%) respectively.~~ This enhanced solar radiation further intensified the heatwaves. Overall, anticyclonic circulation anomalies contributed to air descent and anomalous diabatical heating, resulting in sunny and dry weather in eastern Pamir in July 2022 (Fig. ~~8~~5). This favoured an

555 increase in shortwave radiation to heat the land, which can increase outgoing longwave radiation and turbulent heat fluxes from the land surface to the atmosphere, causing higher air temperatures.

Additionally, soil moisture anomalies and teleconnections via Rossby wave trains (Hood et al., 2020) are also potential contributing factors–. Low soil moisture anomalies on the Tibetan Plateau may have intensified the development of heatwaves through land–atmosphere feedback mechanisms (Jiang et al., 2023). ~~In the summer of 2022, heatwaves swept~~
560 ~~across many parts of the Northern Hemisphere, causing extreme heat events in North America, Europe, and the Yangtze River in China (Lu et al., 2022).~~ The anomalous anticyclone in east Pamir appears to be linked to the propagation of wave energy from an upstream mid-latitude wave train originating in the northwestern North Atlantic (Deng et al., 2023; Song et al., 2024). Anticyclone ~~developed~~ development above western Europe (Fig. ~~11b~~9b) may have acted as a conduit for Rossby wave propagation to the anticyclone developed under the Northwestern flank of ~~TP~~the Tibetan Plateau, linking glacier mass
565 balance in this region to large-scale climate mode such as the Atlantic Multidecadal Oscillation.

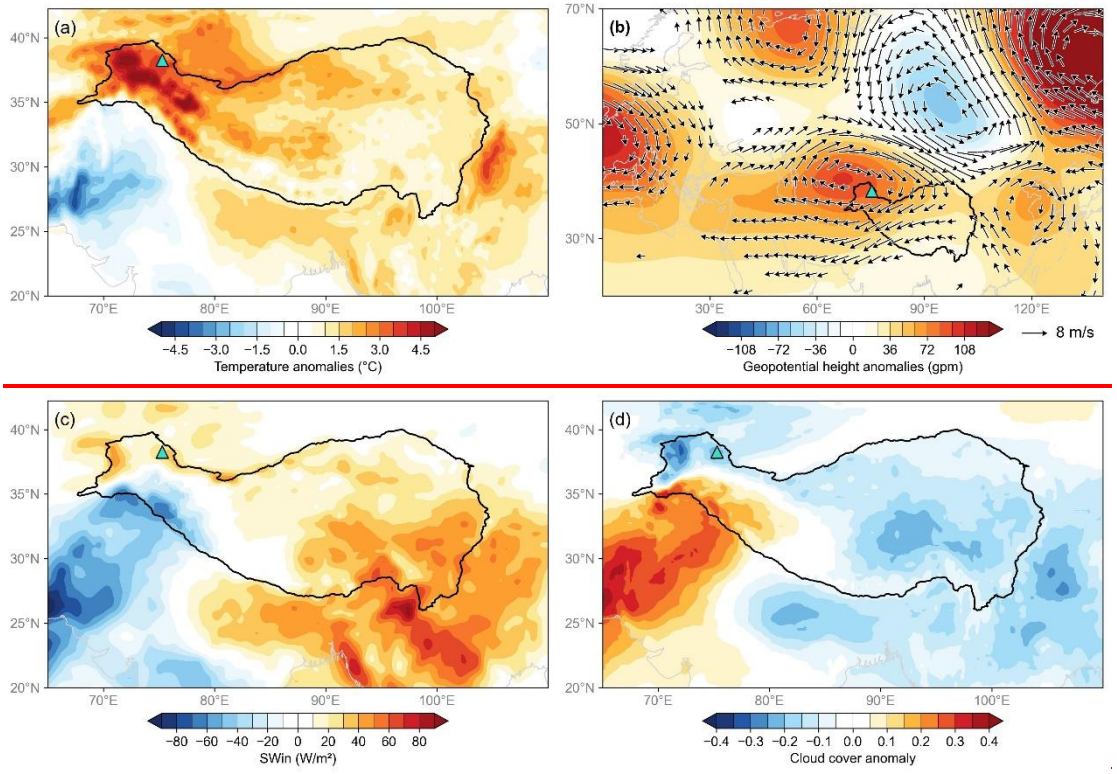

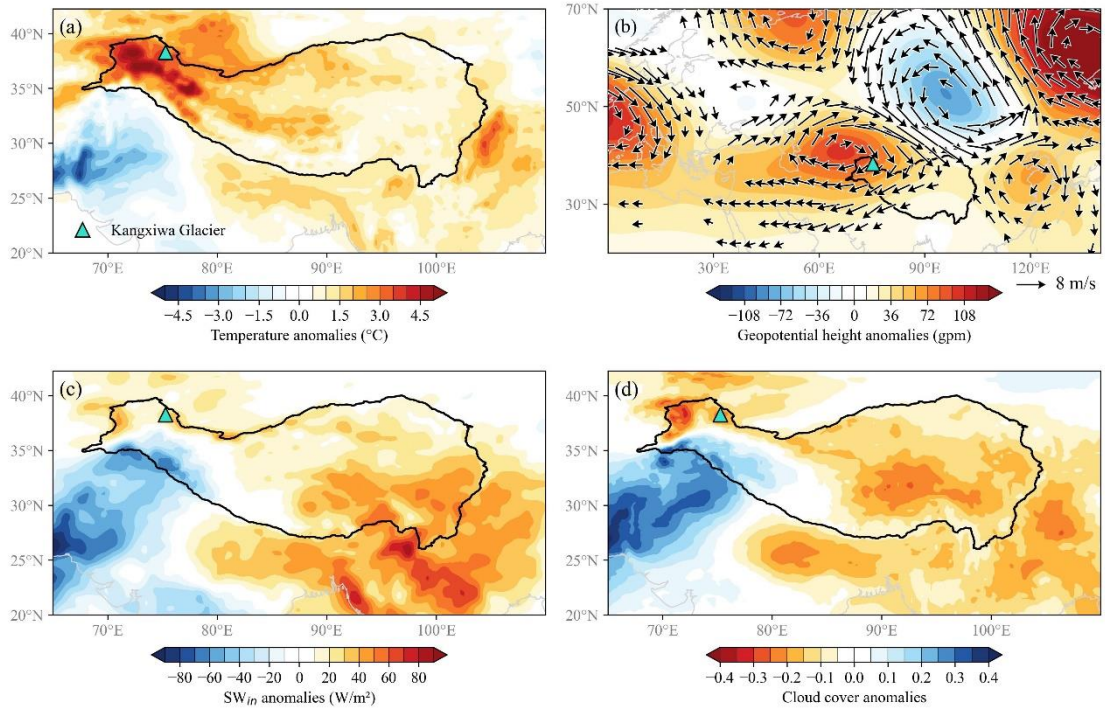

Figure ~~11~~9. The anomalies of meteorological variables and atmospheric circulations in July 2022 compared with climatological (1991-2020) average. (a) Air temperature; (b) Geopotential height (unit: gpm) and wind field anomalies at 200 hpa; (c) Shortwave incoming radiation (SWin, unit: W/m^2) anomaly; (d) Cloud cover fraction anomaly. Black lines represent the domain of the Tibetan Plateau (Zhang et al., 2021)

6. Conclusions

Our study demonstrates that integrating time-lapse camera imagery with in situ glaciological measurements provide~~s~~ a reliable method for quantifying ~~of determining~~ daily surface mass balance of glaciers in the east Pamir region. The results revealed the pronounced interannual variability in the surface mass balance of Kangxiwa Glacier during the 2019/2020-2022/2023 hydrological years: a modest positive balance in 2019/2020, followed by successive negative balances, with a record loss in 2021/2022. High temporal resolution observations ~~e~~characterize eastern Pamir glaciers as~~nable the quantification of accumulation-ablation cycles, generally characterizing regional glaciers in the eastern Pamir~~ as "~~spring~~ spring-accumulation- and ~~summer~~ summer-ablation" type, with accumulation concentrated in ~~mid~~ April–June and ablation in Junely–September. ~~Interannual variability in surface mass balance is predominantly modulated by temperature-driven ablation in summer.~~ Notably, ~~S~~short-term heatwaves could greatly ~~influence~~enhance the ~~considerable~~ mass loss -and then dominate annual ~~SMB~~surface mass balance in this region.~~the Kangxiwa Glacier exhibited~~ experienced ~~considerable mass loss driven by short-term heatwaves~~ extreme sensitivity to heatwaves during relative to over the ablation season.~~ Three heatwaves in July–August 2022 induced over 800 mm w.e. of mass loss within 40 days. ~~This exceptional melting brought~~

forward Coupled with below-average winter–spring accumulation, these heatwavesis advanced the Glacier Loss Day (GLD) by one month in 2022 and ppushed the equilibrium line altitude above the glacier's maximum elevationThe Glacier Loss Day occurred one month earlier in 2022 compared to the other three yearsby one month, due to exceptional melting early in the summer season and/or depleted below-averagespring net accumulation during winter and spring and caused the equilibrium line altitude to rise above the glacier's highest elevation. The 2022 extreme meltevent was linked to weakened westerly circulation over Central Asia, a large-scale atmospheric pattern suppressing moisture transport and amplifying summer warming.affecting Central Asia. Amid global warming and more frequent extreme heat, eastern Pamir glaciers—once considered climate-resilient—face heightened threats to their stability. Our findings clarify their vulnerability to short-term climatic extremes and validate a practical surface mass balance monitoring method for remote mountain regions.Given the recent warming and increasing frequency of the extreme hot weather in East Pamiraround the world, it is possible that glaciers in the eastern Pamir confront substantial challenge.

are transitioning from a state of near-equilibrium or weak negative balance to a state of persistent mass deficit.

References

A2PS contributors: SmartStake: Monitor the glacier ablation with sub-hourly time step and millimetric accuracy, https://a2photonicsensors.com/smartstake-mon (last access: 13 December 2022), 2021.

Barandun, M., and Pohl, E.: Central Asia's spatiotemporal glacier response ambiguity due to data inconsistencies and regional simplifications, The Cryosphere, 17(3), 1343-1371, doi:10.5194/tc-17-1343-2023, 2023.

Barandun, M., Pohl, E., Naegeli, K.,McNabb, R., Huss, M., Berthier, E., Saks, T., and Hoelzle M.: Hot spots of glacier mass balance variability in Central Asia. Geophys. Res. Lett, 48, e2020GL092084. https://doi.org/10.1029/2020GL092084, 2021.

Berthier, E., and Brun, F.: Karakoram geodetic glacier mass balances between 2008 and 2016: persistence of the anomaly and influence of a large rock avalanche on Siachen glacier. J. Glaciol., 65, 251, 494–507. doi: 10.1017/jog.2019.32, 2019.

Berthier, E., Vincent, C., and Six, D.: Exceptional thinning through the entire altitudinal range of Mont-Blanc glaciers during the 2021/22 mass balance year. J. Glaciol., 70, e30, 1-6, https://doi.org/10.1017/jog.2023.100, 2024.

Bhattacharya, A., Bolch, T., Mukherjee, K., King, O., Menounos, B., Kapitsa, V., Neckel, N., Yang, W., and Yao, T.: High Mountain Asian glacier response to climate revealed by multi-temporal satellite observations since the 1960s, Nat. Commun., 12, 4133, https://doi.org/10.1038/s41467-021-24180-y, 2021.

Bolch, T., Shea, J. M., Shiyin, L., Azam, M. F., Gao, Y., Gruber, S., Immerzeel, W. W., Kulkarni, A., Li, H., Tahir, A. A., Zhang, G., and Zhang, Y.: Status and change of the cryosphere in the extended Hindu Kush Himalaya region, in: Wester, P., Mishra, A., Mukherji, A., and Shrestha, A. B. (Eds.), The Hindu Kush Himalaya Assessment, Springer, Cham, 209–255, 2019.

Brun, F., Berthier, E., Wagnon, P., Kääb, A., and Treichler, D.: A spatially resolved estimate of High Mountain Asia glacier mass balances from 2000 to 2016, Nat. Geosci., 10, 668-673, doi:10.1038/ngeo2999, 2017.

Brun, F., Wagnon, P., Berthier, E., Jomelli, V., Maharjan, S. B., Shrestha, F., and Kraaijenbrink, P. D. A.: Heterogeneous influence of glacier morphology on the mass balance variability in High Mountain Asia, J. Geophys. Res. Earth Surf, 124, 1331-1345, https://doi.org/10.1029/2018JF004838, 2019.

Chen, W., Yao, T., Zhang, G., Woolway, R.I., Yang, W., Xu, F., and Zhou, T.: Glacier surface heatwaves over the Tibetan Plateau, Geophys. Res. Lett., 50, e2022GL101115, https://doi.org/10.1029/2022GL101115, 2023.

Cogley, J. G., Hock, R., Rasmussen, L. A., Arendt, A. A., Bauder, A., Braithwaite, R. J., Jansson, P., Kaser, G., Möller, M., Nichol son, L., and Zemp, M.: Glossary of Glacier Mass Balance and Related Terms, IHP-VII Technical Documents in Hydrology No. 86, IACS Contribution No. 2, UNESCO-IHP, Paris, https: //unesdoc.unesco.org/ark:/48223/pf0000192525, 2011.

Cremona, A., Huss, M., Landmann, J. M., Borner, J., and Farinotti, D.: European heat waves 2022: contribution to extreme glacier melt in Switzerland inferred from automated ablation readings, The Cryosphere, 17, 1895–1912, https://doi.org/10.5194/tc-17-1895-2023, 2023.

Colucci, R., Giorgi, F., Torma, C.: Unprecedented heat wave in December 2015 and potential for winter glacier ablation in

the eastern Alps, Sci. Rep., 7: 7090, DOI:10.1038/s41598-017-07415-1, 2017.

Deng, Z., Zhou, S., Wang, M., He, L., Qing, Y., and Qian, Z.: Variations in summer surface air temperature over the eastern Tibetan Plateau: connection with Barents-Kara Spring Sea Ice and Summer Arctic Oscillation, J. Geophys. Res: Atmos, 128, e2023JD039765. https://doi.org/10.1029/2023JD039765, 2023.

Ding, B., Yang K., Qin, J., Wang, L., Chen, Y., and He, X.: The dependence of precipitation types on surface elevation and meteorological conditions and its parameterization. J. Hydrol., 513, 154-163, 2014.

Falaschi, D., Bhattacharya, A., Guillet, G., and Bolch, T.: Annual to seasonal glacier mass balance in High Mountain Asia derived from Pléiades stereo images: examples from the Pamir and the Tibetan Plateau, The Cryosphere, 17, 5435–5458, https://doi.org/10.5194/tc-17-5435-2023, 2023.

Ganesan, P., Rajini, V., Sathish, B. S., and Shaik, K. B.: HSV color space based segmentation of region of interest in satellite images, Proc. Int. Conf. Control Instrum. Commun. Comput. Technol., 101–105, 2014.

Gui, K., Zhou, T., Zhang, W., and Zhang, X.: Land-atmosphere coupling amplified the record-breaking heatwave at altitudes above 5000 meters on the Tibetan Plateau in July 2022, Weather Clim. Extrem., 45, 100717, https://doi.org/10.1016/j.wace.2024.100717, 2024.

Hamuda, E., McGinley, B., Glavin, M., and Jones, E.: Automatic crop detection under field conditions using the HSV colour space and morphological operations, Comput. Electron. Agric., 133, 97–107, https://doi.org/10.1016/j.compag.2016.12.009, 2017.

Hassan, W. U., Nayak, M. A., Saharwardi, M. S., Dar, J. A., Dasari, H. P., Hoteit, I., and Abualnaja, Y.: Unveiling the devastating effect of the spring 2022 mega-heatwave on the South Asian snowpack, Commun. Earth Environ., 5, 707, https://doi.org/10.1038/s43247-024-01857-y, 2024.

Hewitt, K.: Glacier change, concentration, and elevation effects in the Karakoram Himalaya, Upper Indus Basin, Mt. Res. Dev., 31, 188–200, https://doi.org/10.1659/MRD-JOURNAL-D-11-00020.1, 2011.

Hoffmann, L., Günther, G., Li, D., Stein, O., Wu, X., Griessbach, S., Heng, Y., Konopka, P., Müller, R., Vogel, B., and Wright, J.: From ERA‐interim to ERA5: The considerable impact of ECMWF's next‐generation reanalysis on Lagrangian transport simulations. Atmos. Chem. Phys, 19(5), 3097–3124. https://doi.org/10.5194/acp-19-3097-2019, 2019.

Holzer, N., Vijay, S., Yao, T., Xu, J., Buchroithner, M., and Bolch, T.: Four decades of glacier variations at Muztagh Ata (eastern Pamir): a multi-sensor study including Hexagon KH-9 and Pléiades data, The Cryosphere, 9, 2071–2088, https://doi.org/10.5194/tc-9-2071-2015, 2015.

Hood, L. L., Redman, M. A., Johnson, W. L., and Galarneau, T. J.: Stratospheric Influences on the MJO-Induced Rossby Wave Train: Effects on Intraseasonal Climate, J. of Climate, 33, 365-627 389, 10.1175/JCLI-D-18-0811.1, 2020

Hugonnet, R., McNabb, R., Berthier, E., Menounos, B., Nuth, C., Girod, L., Farinotti, D., Huss, M., Dussaillant, I., and Brun, F.: Accelerated global glacier mass loss in the early twenty-first century, Nature, 592, 726–731, https://doi.org/10.1038/s41586-021-03436-z, 2021.

Huss, M.: Density assumptions for converting geodetic glacier volume change to mass change, The Cryosphere, 7, 877–887, 2013.

Huss, M., and Hock, R.: Global-scale hydrological response to future glacier mass loss, Nat. Clim. Change, 8(2), 135-140, doi:10.1038/s41558-017-0049-x, 2018.

Jiang, J., Liu, Y., Mao, J., and Wu, G.: Extreme heatwave over Eastern China in summer 2022: the role of three oceans and local soil moisture feedback. Environ. Res. Lett. 18, 044025. https://doi.org/10.1088/1748-9326/acc5fb, 2023.

Jouberton, A., Shaw, T. E., Miles, E., Kneib, M., Fugger, S., Buri, P., McCarthy, M., Kayumov, A., Navruzshoev, H., Halimov, A., Kabutov, K., Homidov, F., and Pellicciotti, F.: Snowfall decrease in recent years undermines glacier health and meltwater resources in the Northwestern Pamirs. Commun. Earth Environ., 6(1), 691. https://doi.org/10.1038/s43247-025-02611-8, 2025.

Jouberton, A., Shaw, T. E., Miles, E., McCarthy, M., Fug ger, S., Ren, S. T., Dehecq, A., Yang, W., and Pel licciotti, F.: Warming-induced monsoon precipitation phase change intensifies glacier mass loss in the southeastern Tibetan Plateau, P. Natl. Acad. Sci. USA, 119, e2109796119, https://doi.org/10.1073/pnas.2109796119, 2022.

Kääb, A., Leinss, S., Gilbert, A., Bühler, Y., Gascoin, S., Evans, S. G., Bartelt, P., Berthier, E., Brun, F., Chao, W.-A., Farinotti, D., Gimbert, F., Guo, W., Huggel, C., Kargel, J. S., Leonard, G. J., Tian, L., Treichler, D. and Yao, T.: Massive collapse of two glaciers in western Tibet in 2016 after surge-like instability, Nat. Geosci., 11, 114-120, doi:10.1038/s41561-017-0039-7, 2018

Kääb, A., Treichler, D., Nuth, C., and Berthier, E.: Brief Communication: Contending estimates of 2003–2008 glacier mass balance over the Pamir–Karakoram–Himalaya, The Cryosphere, 9, 557–564, https://doi.org/10.5194/tc-9-557-2015, 2015.

Kaser, G., Fountain, A., and Jansson, P.: et al. (2003) A manual for monitoring the mass balance of mountain glaciers. UNESCO, Paris, 2003.

Landmann, J. M., Künsch, H. R., Huss, M., Ogier, C., Kalisch, M., and Farinotti, D.: Assimilating near-real-time mass balance stake readings into a model ensemble using a particle filter, The Cryosphere, 15, 5017–5040, https://doi.org/10.5194/tc-15-5017-2021, 2021.

Li, Z., Wang, N., Chen, A., Zhang, L., and Zhang, Y.: Slight change of glaciers in the Pamir over the period 2000–2017, -Arct. Antarct. Alp. Res., 54, 13–24, https://doi.org/10.1080/15230430.2022.2039766, 2022.

Little, K., Kingston, D., Cullen, N., and Gibson, P.: The role of atmospheric rivers for extreme ablation and snowfall events in the Southern Alps of New Zealand, Geophys. Res. Lett., 46(5), 2761-2771, https://doi.org/10.1029/2018GL081669, 2019.

Liu, W., Zhang, D., Qin, X., van den Broeke, M. R., Jiang, Y., Yang, D., and Ding, M.: Monsoon Clouds Control the Summer Surface Energy Balance on East Rongbuk Glacier (6,523 m Above Sea Level), the Northern of Mt. Qomolangma (Everest). J. Geophys. Res: Atmos, 126, e2020JD033998. https://doi.org/10.1029/2020JD033998, 2021.

Lu, Geman., Li, Qingquan., Sun, Xiaoting., Zhao, Mengchu., Dong, Lili., Wu, Qingyuan., Wang, Lijuan., Zhao, Liang., Duan, Chunfeng., Yin Yizhou., Wang, Pengling., and Shen Xinyong.: Comparative analysis of peak-summer heatwaves in the Yangtze–Huaihe River Basin of China in 2022 and 2013: Thermal effects of the Tibetan Plateau,. Atmos. Res., 300,107222, 2024.

Lu, R., Xu, K., Chen, R., Chen, W., Li, F., Lv, C.: Heat waves in summer 2022 and increasing concern regarding heat waves in general. Atmos. Ocean Sci. Lett., 16, 100290. https://doi.org/10.1016/j.aosl.2022.100290, 2023.

Lv, M., Quincey, D., Guo, H., King, O., Liu, G., Yan, S., Lu, X., and Ruan, Z.: Examining geodetic glacier mass balance in the eastern Pamir transition zone. J. Glaciol., 66, 260, 927-937. https://doi.org/ 10.1017/jog.2020.54, 2020.

Maussion, F., Scherer, D., Mölg, T., Collier, E., Curio, J., and Finkelnburg, R.: Precipitation Seasonality and Variability over the Tibetan Plateau as Resolved by the High Asia Reanalysis, J. Climate, 27, 1910–1927, https://doi.org/10.1175/JCLI-D-13-00282.1, 2014.

Mölg T, Maussion F, and Scherer D.: Mid-latitude westerlies as a driver of glacier variability in monsoonal High Asia. Nat. Clim. Change. 4(1): 68-73. https://doi.org/10.1038/nclimate2055, 2014.

Oliver, E. C. J., Donat, M. G., Burrows, M. T., Moore, P. J., Smale, D. A., Alexander, L. V., Benthuysen, J. A., Feng, M., Sen Gupta, A., Hobday, A. J., Holbrook, N. J., Perkins-Kirkpatrick, S. E., Scannell, H. A., Straub, S. C. and Wernberg, T.: Longer and more frequent marine heatwaves over the past century, Nat. Commun., 9(1), 1324 https://doi.org/10.1038/s41467-018-03732-9, 2018.

Otsu, N.: A Threshold Selection Method from Gray-Level Histograms, IEEE Trans. Syst. Man Cybern., 9, 62–66, https://doi.org/10.1109/TSMC.1979.4310076, 1979.

Perkins-Kirkpatrick, S. E., and Lewis, S. C.: Increasing trends in regional heatwaves, Nat. Commun., 11, 3357, https://doi.org/10.1038/s41467-020-16970-7, 2020.

Ren, Z., Su, F., Xu, B., Xie, Y., and Kan, B.: A coupled glacier hydrology model and its application in eastern Pamir. Journal of Geophysical Research: Atmospheres, 123, 13692–13713. https://doi.org/10.1029/2018JD028572, 2018.

Shean, D. E., Bhushan, S., Montesano, P., Rounce, D. R., Arendt, A., and Osmanoglu, B.: A Systematic, Regional Assessment of High Mountain Asia Glacier Mass Balance, Front. Earth Sci., 7, 363, https://doi.org/10.3389/feart.2019.00363, 2020.

Shi, Y. and Liu, S.: Estimation on the response of glaciers in China to the global warming in the 21st century, Chin. Sci. Bull., 45, 668–672, https://doi.org/10.1007/BF02886048, 2000.

Shugar, D. H., Jacquemart, M., Shean, D., Bhushan, S., and Westoby, M. J.: A massive rock and ice avalanche caused the 2021 disaster at Chamoli, Indian Himalaya, Science, 373, eabh4455, https://doi.org/10.1126/science.abh4455, 2021.

Song, Q., Wang, C., Yao, Y., and Fan, H.: Unraveling the Indian monsoon's role in fueling the unprecedented 2022 Marine Heatwave in the Western North Pacific. npj Clim. Atmos. Sci., 7, 90. https://doi.org/10.1038/s41612-024-00645-x, 2024.

Voordendag, A., Prinz, R., Schuster, L., and Kaser, G.: Brief communication: The Glacier Loss Day as an indicator of a record-breaking negative glacier mass balance in 2022, The Cryosphere, 17, 3661–3665, https://doi.org/10.5194/tc-17-3661-2023, 2023.

WGMS: http://wgms.ch/latest-glacier-mass-balance-data/, WGMS online, available from WGSM, 2025.

Wang R, Liu S, Shangguan D, Radić, V., Zhang, Y.: Spatial heterogeneity in glacier mass-balance sensitivity across High Mountain Asia. Water, 11(4): 776, https://doi.org/10.3390/w11040776, 2019.

Xu, C., Li, H., Wang, F., Li, Z., Zhou, P., and Liu, S.: Heatwaves in summer 2022 forces substantial mass loss for Urumqi Glacier No. 1, China, J. Glaciol., 70, e77, https://doi.org/10.1017/jog.2024.47, 2024.

Yao, T., Bolch, T., Chen, D., Gao, J., Immerzeel, W., Piao, S., Su, F., Thompson, L., Wada, Y., and Wang, L.: The imbalance of the Asian water tower, Nat. Rev. Earth Environ., 3, 618–632, https://doi.org/10.1038/s43017-022-00299-4, 2022.

Yao, T., Thompson, L., Yang, W., Yu, W., Gao, Y., Guo, X., Yang, X., Duan, K., Zhao, H., Xu, B., Pu, J., Lu, A., Xiang, Y., Kattel, D. B., and Joswiak, D.: Different glacier status with atmospheric circulations in Tibetan Plateau and surroundings, Nat. Clim. Change, 2, 663–667, https://doi.org/10.1038/nclimate1580, 2012.

Yu, L., Chou, S., Wu, H., Chen, Y., and Chen, Y.: Rapid and semi-quantitative colorimetric loop-mediated isothermal amplification detection of ASFV via HSV color model transformation, J. Microbiol. Immunol. Infect., 54, 963–970, https://doi.org/10.1016/j.jmii.2020.08.003, 2021.

~~Yu, W., Yao T., Kang, S., Pu J., Yang W., Gao T., Zhao H., Zhou, H., Li, S., Wang, W., and Ma, L.: Different region climate regimes and topography affect the changes in area and mass balance of glaciers on the north and south slopes of the same glacierized massif (the West Nyainqentanglha Range, Tibetan Plateau), J. Hydrol., 495(2013), 64-73, 2013.~~

Zemp, M., Gärtner-Roer, I., Nussbaumer, S. U., Welty, E. Z., Dussaillant, I., and Bannwart, J. (Eds.): Global Glacier Change Bulletin No. 5 (2020–2021), ISC(WDS)/IUGG(IACS)/UNEP/UNESCO/WMO, World Glacier Monitoring Service, Zurich, Switzerland, 134 pp., ISBN: 978-3-033-10025-5, https://doi.org/10.5904/wgms-fog-2023-09, 2023.

Zhang, T., Deng, G., Liu, X., He, Y., Shen, Q., and Chen Q.: Heatwave magnitude quantization and impact factors analysis over the Tibetan Plateau. npj Clim. Atmos. Sci., 8, 2, https://doi.org/10.1038/s41612-024-00877-x, 2025.

Zhang, Y., Li, B., Liu, L., and Zheng, D.: Redetermine the region and boundaries of Tibetan Plateau, Geogr. Res., 40(6), 1543-1553, doi:10.11821/dlyj020210138 cstr:32071.14.dlyj020210138, 2021 (in Chinese with English abstract).

Zhao, C., Yang, W., Westoby, M., An, B., Wu, G., Wang, W., Wang, Z., Wang, Y., and Dunning, S.: Brief communication: An approximately 50 Mm³ ice-rock avalanche on 22 March 2021 in the Sedongpu valley, southeastern Tibetan Plateau, The Cryosphere, -16, 1333–1340, https://doi.org/10.5194/tc-16-1333-2022, 2022.-

Zhu, F., Zhu, M., Guo, Y., and Yao, T.: Observation and simulation of runoff during an extreme heatwave in a glacial basin on the Central Tibetan Plateau, Hydrol. Process., 38, e70014, https://doi.org/10.1002/hyp.70014, 2024a.

Zhu, F., Zhu, M., Yang, W., Wang, Z., Guo, Y., and Yao, T.: Drivers of the extreme early spring glacier melt of 2022 on the central Tibetan Plateau, Earth Space Sci., 11, e2023EA003297, https://doi.org/10.1029/2023EA003297, 2024b.

Zhu, M., Thompson, L. G., Yao, T., Jin, S., Yang, W., Xiang, Y., and Zhao, H.: Opposite mass balance variations between glaciers in western Tibet and the western Tien Shan. Global Planet. Change, 220, 103997. https://doi.org/10.1016/j.gloplacha.2022.103997, 2023.

Zhu, M., Yao, T., Yang, W., Xu, B., Wu, G., and Wang, X.: Reconstruction of the mass balance of Muztag Ata No. 15 glacier, eastern Pamir, and its climatic drivers, J. Glaciol., 64, 259–274, https://doi.org/10.1017/jog.2018.22, 2018.

Acknowledgement

The study was supported by the National Key R&D Program of China (Grant No. 2024YFF0808601), National Natural Science Foundation of China (Grant No. 422711382), Excellent Research Group Program for Tibetan Plateau Earth System (No. 42588201), Lhasa Science and Technology Plan Project (LSKJ202406), ~~the National Key R&D Program of China (Grant No. 2024YFF0808601),~~ Science and Technology Plan Projects of Tibet Autonomous Region (XZ202301ZY0022G), Key Innovation Team of National Climate Centre "Climate Change Monitoring and Projection in the Third Pole Region" (NCCCXTD007).

Code and data availability

Data in this study are available upon request from the corresponding author.

Author contributions

X.Y., W.Y analysed the data and write the manuscript. M.Z.,Y.F., S.Y., P.W., W.Z. assisted in collecting all data and discussion. Funding acquisition, W.Y., B.X. All authors have read and agreed to the published version of the manuscript.

Competing interests

The authors declare that they have no conflict of interests.

Disclaimer. Publisher's note: Copernicus Publications remains neutral with regard to jurisdictional claims in published maps and institutional affiliations.

Supplementary Figures

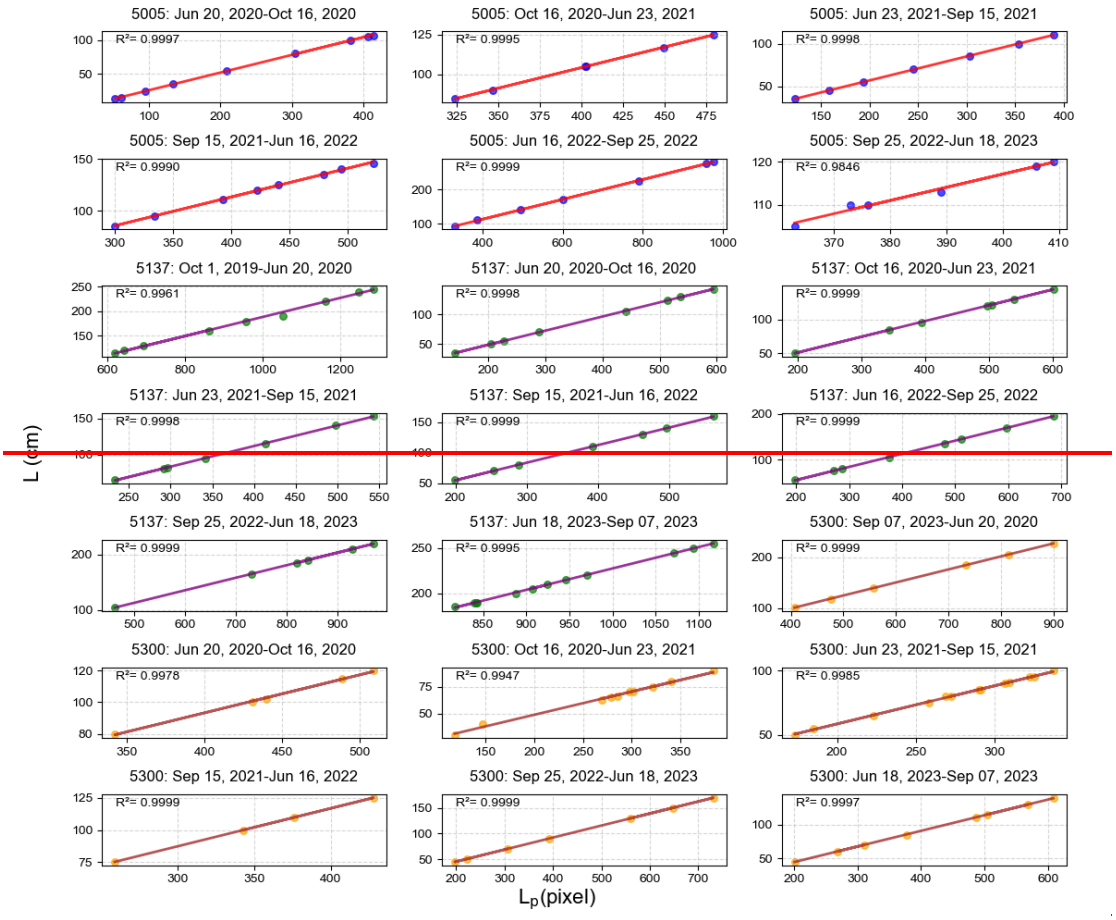

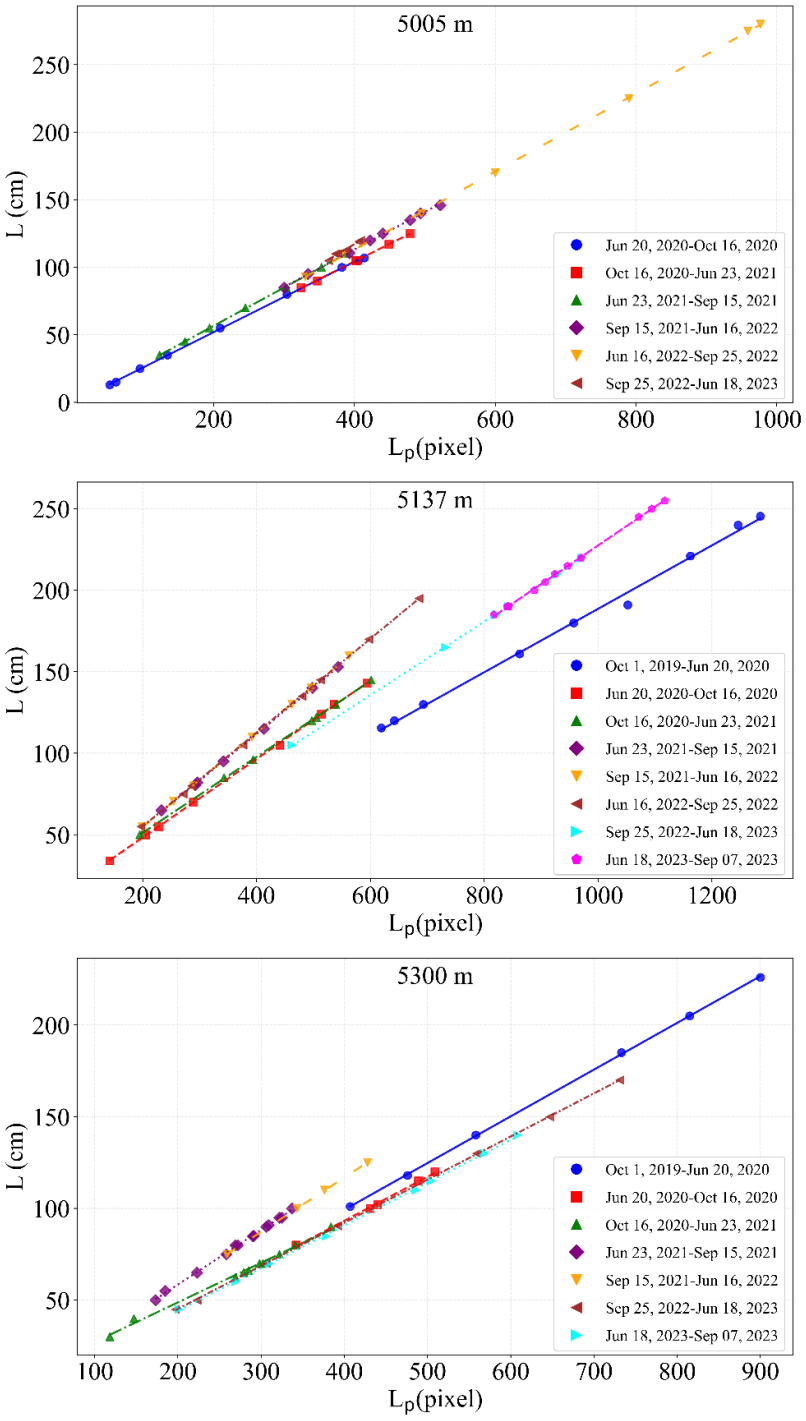

790

Figure S1 Linear relationship between L_p and L for each monitoring period at each ~~monitoring~~ camera site.

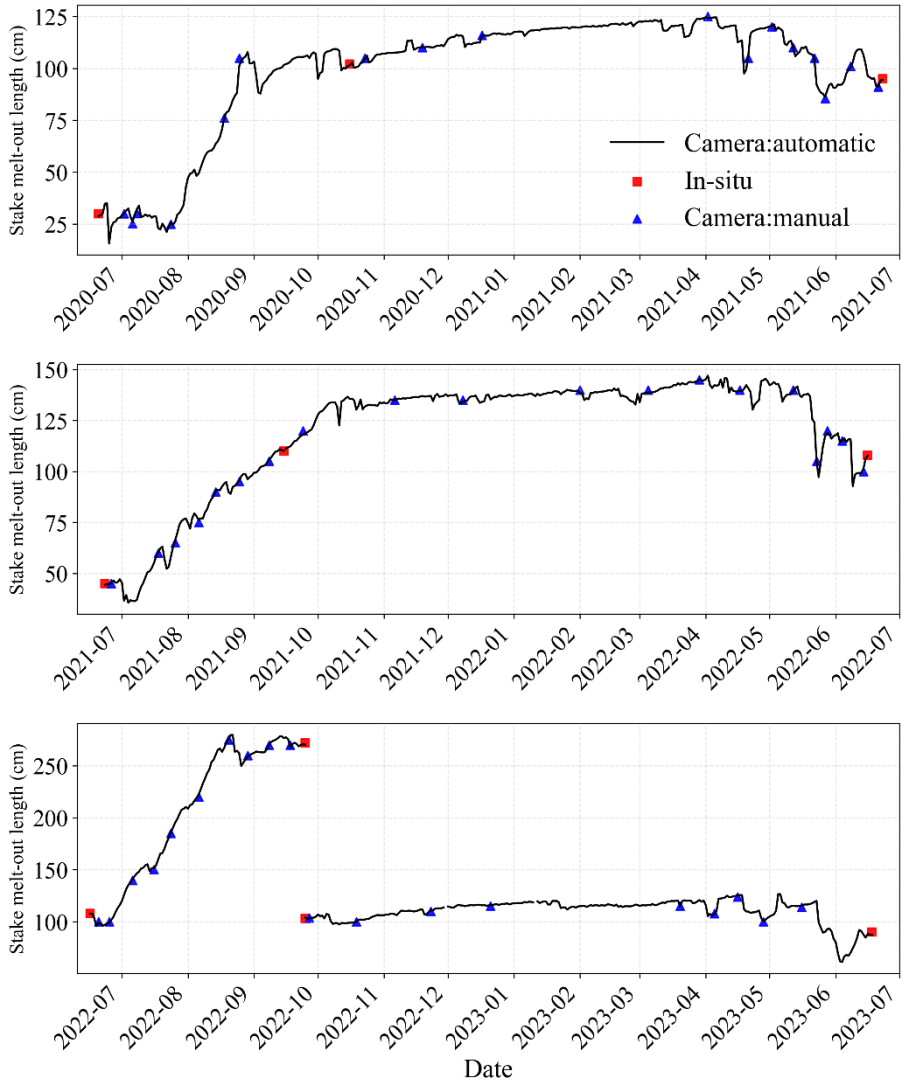

Figure ~~3~~S2. The performance of stake melt-out lengths~~changes~~ derived automatically from time-lapse cameras (black line), compared with in-situ observations (red square) and manual ~~calculation~~inspections (blue triangle) for a stake at the elevation of 5005 m asl. Noted that the camera monitoring systems were maintained in June and September in each year during the period from 2020 to 2023.

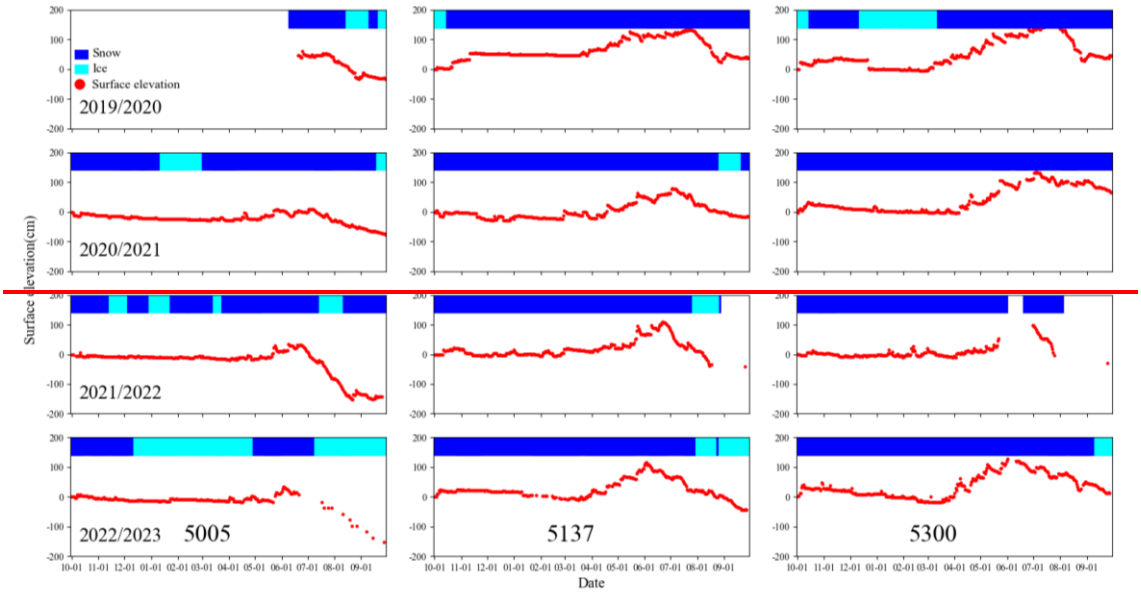
Snow
Ice
Surface elevation
2019/2020
2020/2021
2021/2022
2022/2023
5005
5137
5300
Surface elevation(cm)
Date

800

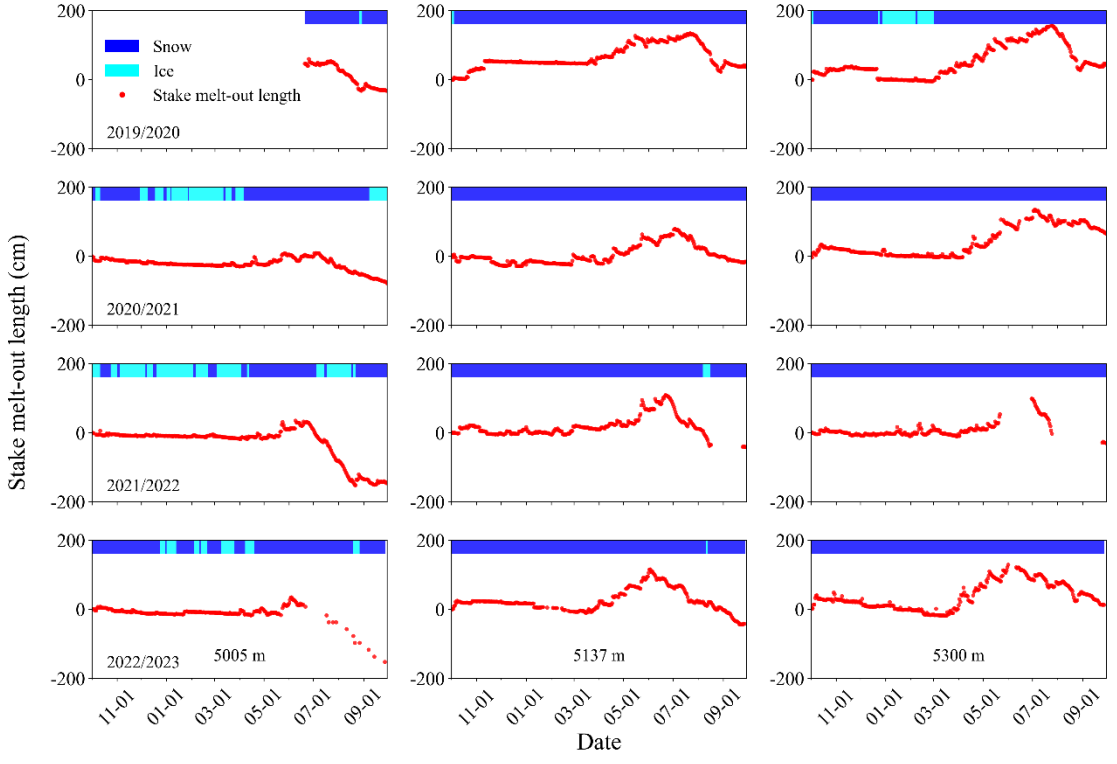
Snow
Ice
Stake melt-out length
2019/2020
2020/2021
2021/2022
2022/2023
5005 m
5137 m
5300 m
Stake melt-out length (cm)
Date

Figure S3 Changes in stake melt-out length derived by subtracting all data from the baseline values recorded on the first day of each hydrologic year ~~The surface elevation changes at three locations~~ on the Kangxiwa Glacier and ~~their~~ evolutions of snow and bare ice surface conditions over the hydrological years 2019/2020 to 2022/2023.

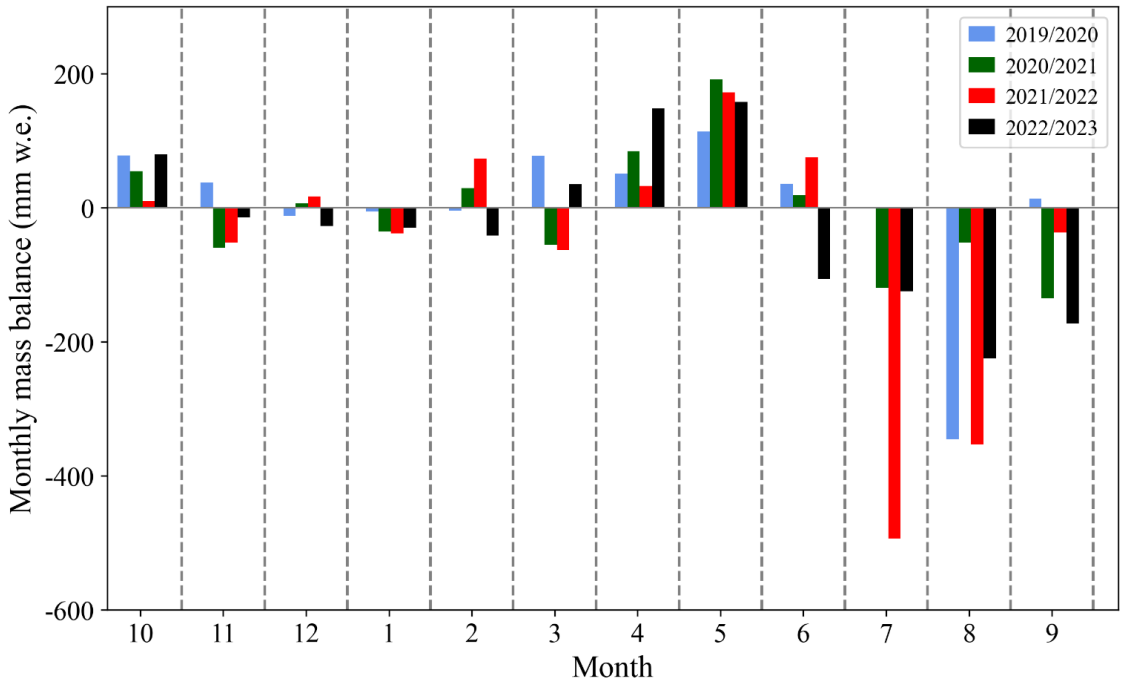

Figure S4 Comparison of monthly glacier mass balance of Kangixwa Glacier between four hydrological years of 2019/2020-2022/2023.

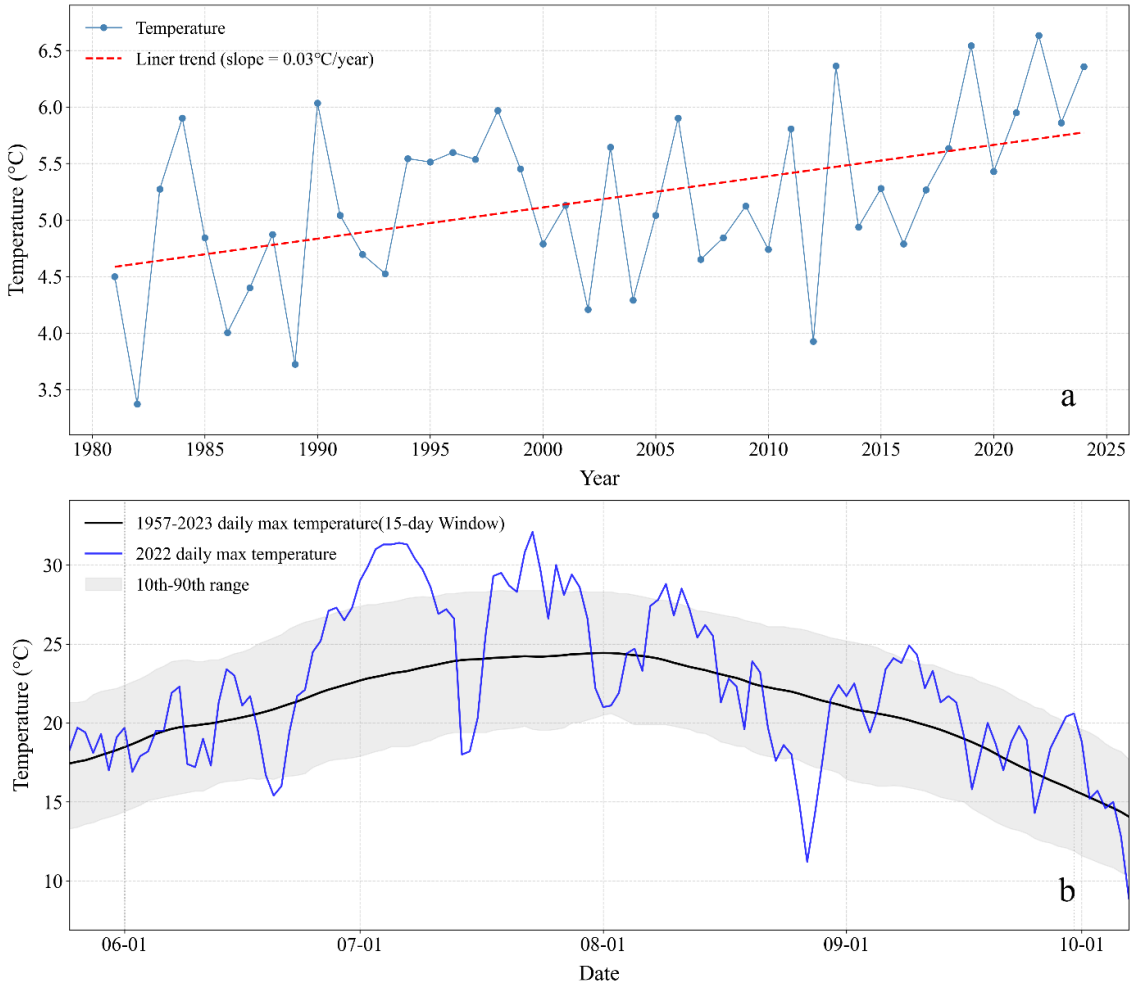

Figure ~~S3~~ S5 Variation of mean E~~A~~RA-land air temperature in July (a) and July-September (b) at the corresponding grid point of Kangxiwa Glacier during the period from 1981 to 2024. (c) Comparison of June-September daily max air temperature in 2022 with the 1957-2023 mean at Taxkorgan station.

820